Sedimentary Geology 442 (2022) 106290

Contents lists available at ScienceDirect

Sedimentary Geology

journal homepage: www.elsevier.com/locate/sedgeo

Unraveling an alkaline lake and a climate change in Northeastern Brazil during the Late Aptian

Victor Matheus Joaquim Salgado-Campos [a,b,c,f,*], Ismar de Souza Carvalho [a,e], Luiz Carlos Bertolino [c,d], Leonardo Borghi [a,b], Aristóteles de Moraes Rios-Netto [a], Bruno Cesar Araújo [a,b], Danielle Cardoso de Souza [a,b], Laís de Oliveira Ferreira [a,b], Fabia Emanuela Rafaloski Bobco [a,b]

[a] Universidade Federal do Rio de Janeiro, Instituto de Geociências, Departamento de Geologia, Av. Athos da Silveira Ramos, 274-21941-909, Cidade Universitária, Rio de Janeiro, RJ, Brazil
[b] Universidade Federal do Rio de Janeiro, Instituto de Geociências, Departamento de Geologia, Laboratório de Geologia Sedimentar, Av. Athos da Silveira Ramos, 274-21941-909, Cidade Universitária, Rio de Janeiro, RJ, Brazil
[c] Centro de Tecnologia Mineral, Coordenação de Análises Minerais, Setor de Caracterização Tecnológica, Av. Pedro Calmon, 900-21941-908, Cidade Universitária, Rio de Janeiro, RJ, Brazil
[d] Universidade do Estado do Rio de Janeiro, Faculdade de Geologia, Departamento de Mineralogia e Petrologia Ígnea, Rua São Francisco Xavier, 524 – 20550-000, Maracanã, Rio de Janeiro, RJ, Brazil
[e] Universidade de Coimbra, Centro de Geociências, Rua Sílvio Lima, Pólo II, 3030-709 Coimbra, Portugal
[f] Universidade Federal Fluminense, Instituto de Geociências, Departamento de Geologia e Geofísica, Av. Gal. Milton Tavares de Souza, s/n°, 24210-346, Gragoatá, Niterói, Rio de Janeiro, Brazil

ARTICLE INFO

Article history:
Received 13 September 2022
Received in revised form 1 November 2022
Accepted 2 November 2022
Available online 10 November 2022

Editor: Dr. Massimo Moretti

Keywords:
Codó Formation
Alkaline lake
Saponite
Climate change
Aptian

ABSTRACT

The Codó Formation is an Aptian marine-influenced lacustrine depositional system in the Parnaíba Basin (Brazil). This unit is an important sedimentary succession because of the high organic matter content and for being an ancient analog for the depositional systems of the Brazilian Pre-salt interval. However, mineralogical and lithogeochemical studies have not been sufficiently carried out on the Codó Formation, which hinders detailed sedimentological knowledge. We report new mineralogical and lithogeochemical data that allow a better understanding of the environmental, climatic, and provenance evolution of the Codó deposits. Mineralogical and lithogeochemical studies were performed on 50 lutite samples collected from the 1-UN-32-PI core and 13 outcrop lutite samples obtained from sites close to the Grajaú and Imperatriz regions. A magnesium-sulfate-rich shallow alkaline hypersaline lake was identified in the lower Codó Formation based on the identification of a clay mineral assemblage composed of authigenic saponite and detrital illite. Hydrothermal processes were interpreted as the magnesium source of this alkaline lake. A salinity-alteration event was identified at the upper limit of the alkaline lake and was interpreted as the first marine ingression in the Codó Formation. This event changed the lake's pH from alkaline to acid, inhibiting the formation of Mg-smectites, and changing its hydrochemical conditions, originating a marine-influenced sulfate-rich acid saline/hypersaline sabkha. This facies succession coincides with a clay mineral assemblage composed of detrital montmorillonite, illite and kaolinite. A regional paleoclimate humidification process was identified from the sabkha to a lagoon facies succession in the upper Codó Formation. This last succession reveals the marine-dominated interval of the Codó Formation and coincides with a clay mineral assemblage composed of detrital kaolinite, montmorillonite and illite. Based on lithogeochemical data, a common post-Archean intermediate source area was also interpreted for these three environments.

1. Introduction

In order to study modern and ancient sedimentary environments, clay mineralogy and lithogeochemistry have been widely applied (Hussain et al., 2021; Craigie, 2018; Weaver, 1989; Chamley, 1989). Depending on the genesis (detrital or authigenic) of clay mineral assemblages, different sedimentological information can be obtained.

Detrital clay mineral assemblages originated from sedimentological processes involving weathering, erosion, transportation and deposition in sedimentary environments (Wunderlin et al., 2022; Thiry, 2000; Weaver, 1989; Singer, 1984a; Barshad, 1966). These clay mineral assemblages can be used for paleoclimatic and provenance reconstructions because their composition is controlled mainly by source-area lithology and source-area climates. In this sense, wet climates produce kaolinite-rich soils (e.g., argisols), while dry climates generate

* Corresponding author at: Universidade Federal do Rio de Janeiro, Instituto de Geociências, Departamento de Geologia, Av. Athos da Silveira Ramos, 274-21941-909, Cidade Universitária, Rio de Janeiro, RJ, Brazil.
E-mail address: vsalgado@id.uff.br (V.M.J. Salgado-Campos).

https://doi.org/10.1016/j.sedgeo.2022.106290
0037-0738/

smectite-rich soils (e.g., gleysols) (Carbonell et al., 2022; Velde and Meunier, 2008; Chamley, 1989).

Authigenic clay mineral assemblages are formed in situ in response to specific physical–chemical conditions and can be used for paleoenvironmental reconstructions (Pozo and Calvo, 2018; Meunier, 2005). A wide range of genesis can be stated for this type of clay mineral assemblage, this being formed (1) syngenetically in saline or hypersaline sedimentary environments; (2) diagenetically involving post-depositional fluids and their interaction with host rocks; or (3) telodiagenetically through the weathering of sedimentary rocks exposed to subaerial conditions.

This study was carried out in the Codó Formation, a 150-meter-thick succession of lutites, laminated limestones, evaporites (gypsum) and sandstones that composes part of the late Aptian record of the Parnaíba Basin, an intracratonic sedimentary basin in Northeastern Brazil (Fig. 1) (Vaz et al., 2007; Góes and Feijó, 1994; Fernandes and Piazza, 1978; Campbell, 1949; Lisboa, 1914). This formation has been historically considered either a lacustrine or a restricted depositional system with marine influence (Bastos et al., 2020; Bahniuk et al., 2015; Paz et al., 2005; Rossetti et al., 2004; Antonioli, 2001; Rodrigues, 1995; Cerqueira and Marques, 1985; Mesner and Wooldridge, 1962, 1964; Fernandes and Piazza, 1978; Leite et al., 1975; Rezende and Pamplona, 1970) and has been receiving attention because of the high organic matter content possibly associated with anoxic events (Bastos et al., 2020; Sousa et al., 2019; Rodrigues, 1995; Cerqueira and Marques, 1985). Furthermore, it is considered an ancient analog to the rocks of the giant oil reserves in the Brazilian marginal basins known globally as the Pre-salt succession (Netto et al., 2022; Wright, 2020; Bahniuk et al., 2015; Maizatto et al., 2011) being associated with the Gondwana breakup (Richetti et al., 2018; Dietz and Holden, 1970).

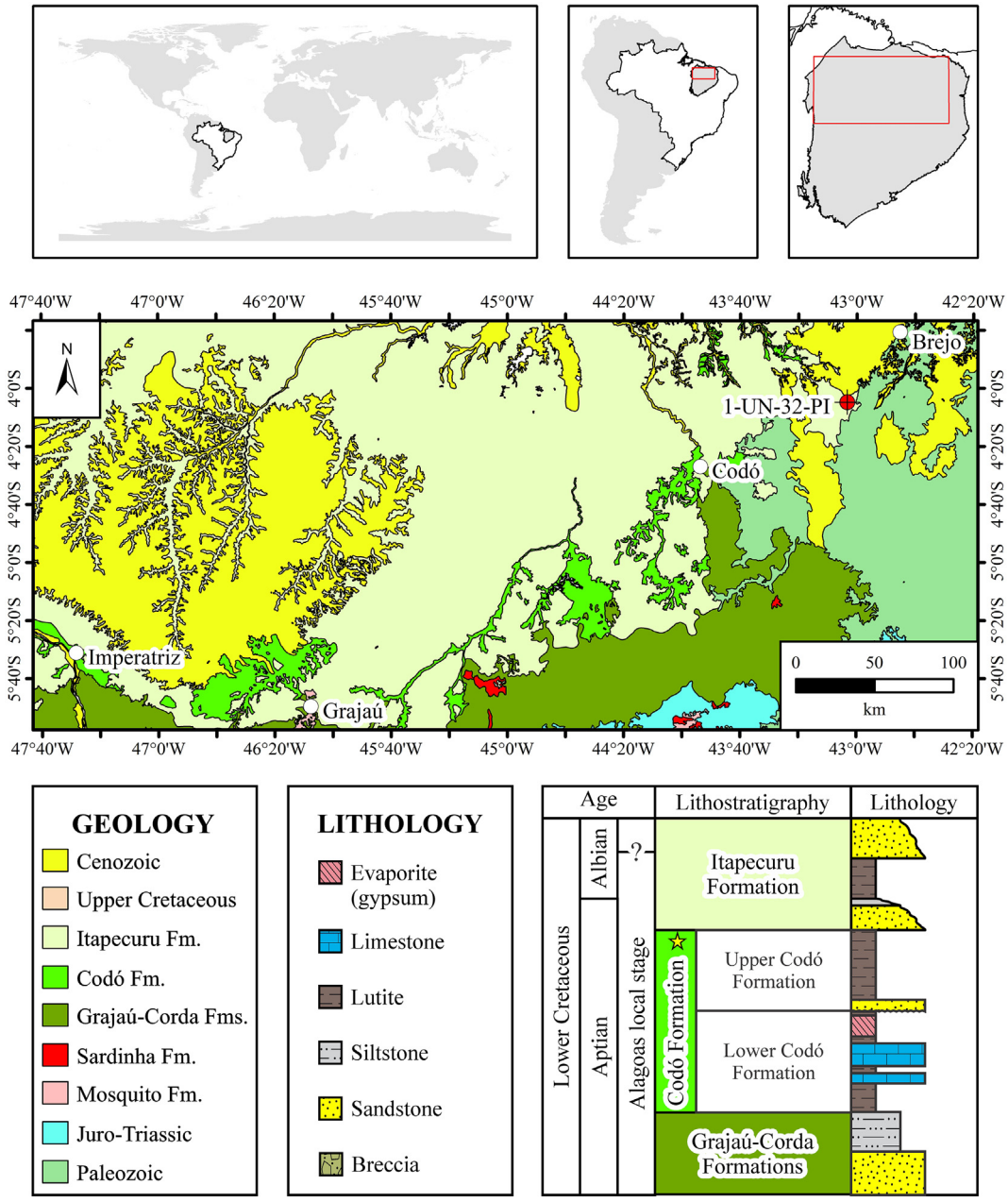

Fig. 1. Geological map and stratigraphic section of the studied area (Vasconcelos et al., 2004). Góes and Feijó (1994) was used as lithostratigraphy and Mendes (2007) and biocronostratigraphy were obtained from Regali and Santos (1999) and Ferreira et al. (2020). 1-UN-32-PI (4° 4′55.00″S 43° 3′15.00″W), Chorado 1 (C1) and Chorado 3 (C3) (5°46′22.40″S; 46°7′24.19″W), Calcário Grajaú (CG) (5°44′18.20″S; 46° 6′59.08″W) and Imperatriz (IM) (5°34′38.47″S; 47°29′13.20″W).

Previous studies have indicated that the clay mineral assemblages of the Codó Formation lutites are composed mainly of montmorillonite, illite and kaolinite, with minor occurrences of palygorskite, which indicates a semiarid to arid climate (Gonçalves et al., 2006; Rossetti et al., 2001). This information has been corroborated by lithological (evaporite) and paleontological data (Boucot et al., 2013; Hay and Floegel, 2012; Skelton et al., 2003; Chumakov et al., 1995; Petri, 1983; Lima, 1983).

However, this Brazilian Aptian unit's paleoenvironmental and -climate evolution remains poorly understood and sophisticated studies using clay mineralogy and lithogeochemistry would help shed light on its geological evolution. In this sense, we report new mineralogical and lithogeochemical data from the Codó Formation (Parnaíba Basin) regarding its paleoenvironmental, -climatic, and provenance reconstructions in Northeastern Brazil during the late Aptian (Early Cretaceous).

2. Geological settings

The Codó Formation covers an area of 170,000 km^2, is overlain by an erosive unconformity with the Itapecuru Formation and is underlain by the Grajaú or Corda formations (Lima, 1983; Fernandes and Piazza, 1978; Rezende and Pamplona, 1970). The Codó Formation can be separated into the lower and upper Codó Formation, which are bounded by an unconformity located at the base of an approximately 5-meter-thick sandstone bed (Fig. 2) (Mendes, 2007). Numerous authors have attributed the Codó Formation to the P-270 and P-280 palynozones (Antonioli, 2001; Pedrão et al., 1993), which is correlated to the late Aptian (Alagoas local state) (Regali and Santos, 1999).

The marine influence on the Codó Formation also remains a key point to understand its depositional system. The lack of marine fossils and abundant lacustrine fossiliferous records (e.g., continental

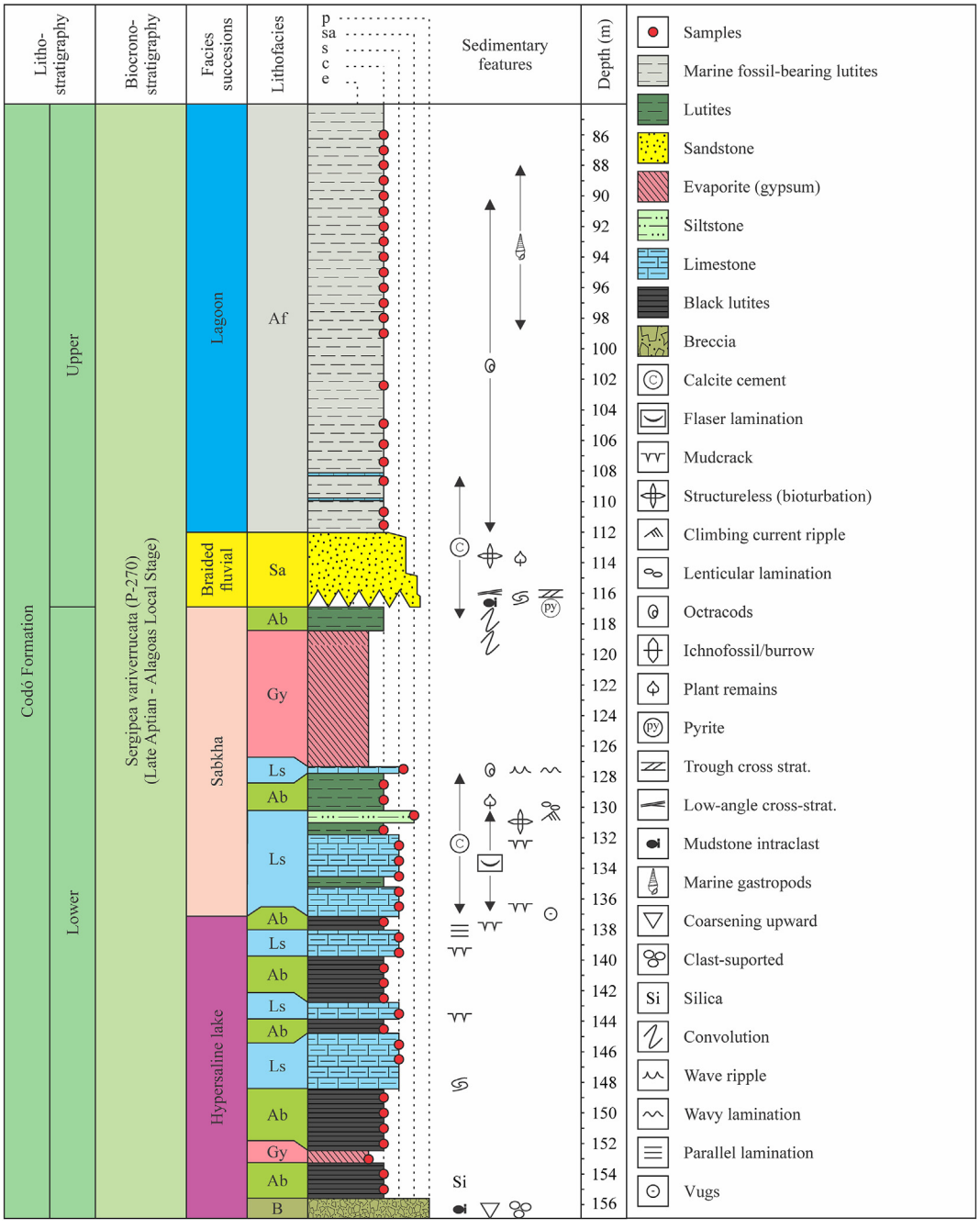

Fig. 2. Lithological profile of the Codó Formation in the 1-UN-32-PI well (modified from Mendes, 2007). e – evaporite; c – clay; s – silt; sa – sand; p – pebble.

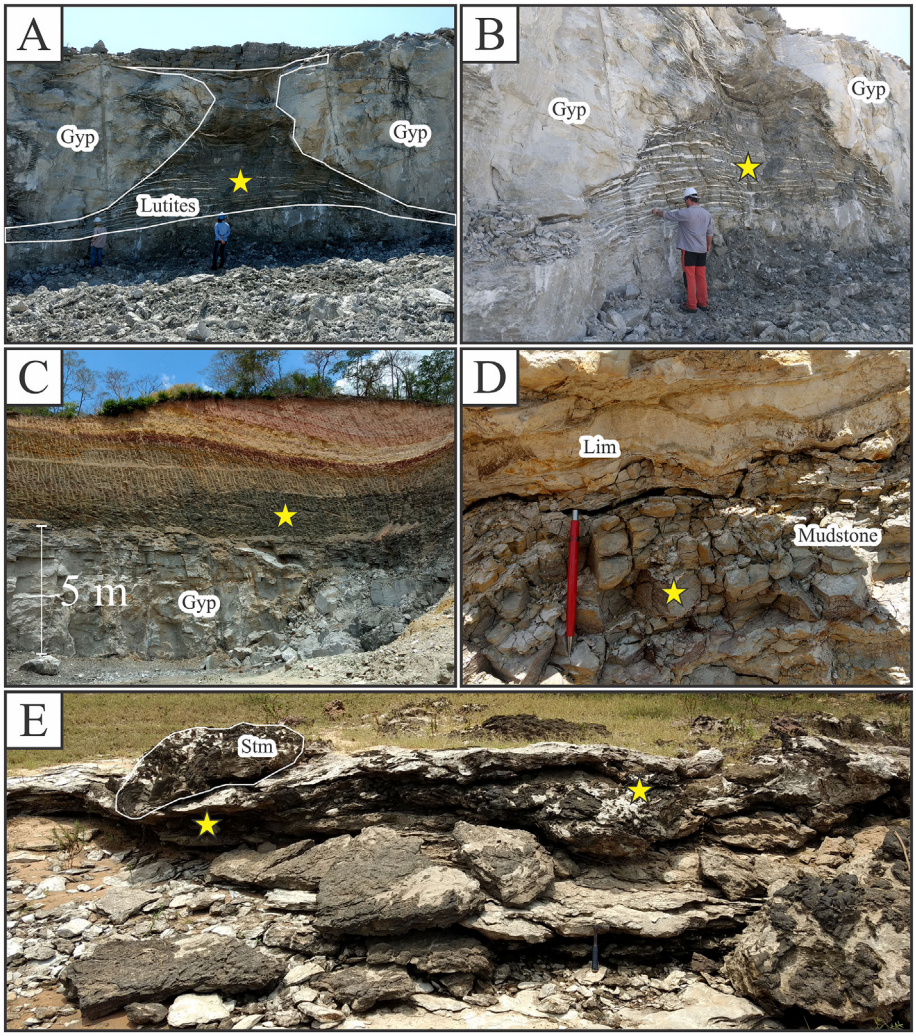

Fig. 3. Outcrops in the Grajaú and Imperatriz area. Star – Sample site. Gyp - gypsum, Lim – limestone and Stm – stromatolite. A) Bedset of lutites deformed by gypsum beds in the Chorado 1 quarry. B) Detailed image of the sampling site in the Chorado 1 quarry. C) Overview of the sampling site in the Chorado 3 quarry. D) Sampling site in the Calcário Grajaú quarry. E) Praia das Gaivotas outcrop in the Imperatriz region.

ostracods) in the Grajaú area reinforces continental sedimentation (Paz and Rossetti, 2001). However, paleontological evidence, including echinoderm spines and marine palynomorphs (e.g., dinoflagellates), has been found in the Codó area, indicating a marine contribution (Lindoso et al., 2013, 2016; Antonioli, 2001; Pedrão et al., 1993), as corroborated by the marine seaway model advocated by Arai (2014).

Diverse lithofacies analyses have been performed in the Codó Formation using outcrop and core samples (Paz et al., 2005; Rossetti et al., 2004; Paz and Rossetti, 2001), being one of the most important conducted by Mendes (2007), who investigated four cores from the Carvão Project, including the one studied here. The author proposed six lithofacies: three clastic, two chemical, and one breccia (Fig. 2). The two lutite lithofacies comprise bituminous lutites with mudcracks interlaminated with gypsum and calcite (Ab) and fossiliferous lutites with ostracods and marine gastropods (Af). The sandstone lithofacies comprises a fining-upward bed of fine to medium-grained sandstone with wavy or flaser bedding (Sa). Finally, the two chemical lithofacies include limestone (Ls) and gypsum bedsets (Gy). A bed of intraformational breccia (B) composes the breccia lithofacies.

Mendes (2007) also proposed four different facies associations based on sedimentological and paleontological data. A hypersaline lake followed by a sabkha depositional system was attributed to the lower Codó Formation, including the evaporite bed, whereas a braided fluvial followed by a marine-influenced lacustrine depositional system (lagoon) was interpreted in the upper Codó Formation.

Table 1
Structures used in the quantitative mineral analyses. COD - Crystallographic Open Database; ICDD - International Centre for Diffraction Data (PDF-4+).

Structure	Code	Reference
Montmorillonite	COD 900277	Viani et al. (2002)
Palygorskite	COD 9005565	–
Gypsum	ICDD 00-036-0432	–
Muscovite	ICDD 04-015-8226	Brigatti et al. (2008)
Kaolinite	ICDD 00-014-0164 (BISH)	Goodyear and Duffin (1961)
Bassanite	ICDD 00-041-0224	–
Aragonite	ICDD 00-041-1475	–
Quartz	ICDD 00-046-1045	Kern and Eysel (1993)
Microcline	ICDD 00-019-0926	Technisch Physiscge Dienst (1966)
Albite	ICDD 00-078-1995	–
Calcite	–	Santos et al. (2017)
Dolomite	–	Santos et al. (2017)
Barite	–	–
Pyrite	ICDD 00-006-0710	–

Table 2
Diagnostic reflections (Å) used in the mineralogical characterization.

Mineral	Bulk mineralogy	Clay mineralogy			
		Air-dried	Ethylene-glycol solvated	Heated at 550 °C	*d*060
Saponite	–	15	17	10	1.525
Montmorillonite	–	15	17	10	1.50
Palygorskite	–	10.5	10.5	–	–
Illite	–	10	10	10	1.50
Kaolinite	–	7	7	–	1.49
Illite-smectite mixed layered clay minerals	–	–	8.5/5.5	–	–
Gypsum	7.59	–	–	–	–
Bassanite	6.00	–	–	–	–
Quartz	4.25/3.34	–	–	–	1.82/1.54
Aragonite	3.39	–	–	–	–
Calcite	3.03/3.00	–	–	–	–
Dolomite	2.90	–	–	–	–
K-feldspar	3.24	–	–	–	–
Plagioclase	3.18	–	–	–	–
Pyrite	2.70	–	–	–	–

3. Materials and methods

3.1. Sampling sites

Fifty lutite samples were collected along the 1-UN-32-PI core, which was drilled in the 1970s during a government program called Projeto Carvão, aiming to discover coal beds (Leite et al., 1975). A total of ten samples were also collected in three different outcrops near the Grajaú area, which comprises the Chorado 1, Chorado 3, and Calcário Grajaú quarries, while three samples were collected from the Imperatriz outcrop (IM), also known as the Praia da Gaivota outcrop, near the city of Imperatriz (Fig. 1).

The Chorado 1 and 3 quarries occur between and above packages of gypsum, respectively, and are composed of a succession of lutites interbedded with evaporites (Fig. 3A, B and C). The Calcário Grajaú outcrop is composed of a bed of lutites underneath a limestone bed (Fig. 3D). The Imperatriz outcrop is located along the Tocantins River and comprises lutites associated with stromatolites (Fig. 3E) (Bahniuk et al., 2015; Coura, 2011).

3.2. Methods

X-ray diffractometry, scanning electron microscopy and X-ray fluorescence were performed at the Center for Mineral Technology (Brazil). Bulk samples were dehydrated at 60 °C for 24 h and processed in a ball mill using an agate media in cycles at 300 RPM for 5 min to obtain a sample size of <106 μm. Fractions were decarbonated using a buffered solution of acetic acid (2 M) and sodium acetate (2 M) heated at 80 °C (Coimbra et al., 2021; Carrado et al., 2006). Stokes' law was applied to obtain the clay-sized fraction (<2 μm) (Moore and Reynolds, 1997). These processes were carried out for clay mineral analysis. Other aliquots were pulverized in a McCrone mill (<10 μm) using water and an agate recipe for quantitative mineral analysis (Rietveld method).

Qualitative clay mineral analyses were conducted using air-dried, ethylene-glycol solvation for 16 h and heating at 550 °C for 2 h on oriented glass slides (Brindley and Brown, 1980). The method of Christidis and Koutsopoulou (2013) was used to determine Mg-smectite species. These diffraction patterns were acquired using the Bruker-AXS D8 Advance ECO diffractometer using dynamic beam optimization (DBO) in the 2θ range from 1 to 40° with a scan velocity of 0.01°/s.

Reflections at 1.54 Å in random mounted samples were compared with reflections at 1.82 Å to determine if that reflection is associated with trioctahedral clay minerals. A Bruker-AXS D8 Advance ECO diffractometer was used to acquire these diffractograms, which were obtained in the 2θ range from 4 to 70° with a scan velocity of 0.02°/s. Quantitative clay mineral analyses were performed using the method of Biscaye (1965). Due to methodological issues, samples located at 112.00 and 109.65 m were not studied for clay mineralogy.

The Rietveld method (Young, 1993; Cheary and Coelho, 1992) was applied to perform quantitative mineral analyses on bulk fractions using Bruker-AXS D4 Endeavor equipment using a LynxEye position-sensitive detector operating at 40 kV and 40 mA with CoKα radiation (λ = 1.78897 Å) and Bruker-AXS D8 Advance ECO equipment using a LynxEye XE energy-discriminant position-sensitive detector operating at 40 kV and 25 mA with CuKα radiation (λ = 1.54060 Å). The diffractograms were obtained in the 2θ range from 4 to 105° with a scan velocity of 0.02°/s. The bulk samples in the interval from 155.00 to 137.50 were studied in the Bruker-AXS D4 diffractometer, while the samples in the interval from 136.50 to 86.00 m and the outcrop samples were studied in the Bruker-AXS D8 equipment.

Quantitative mineral analyses were performed with a Bruker-AXS TOPAS v5 device using the Crystallographic Open Database (COD) and the International Centre for Diffraction Data (PDF-4+) (ICDD) databases, in which the structures can be found in Table 1. Warr (2020) and Whitney and Evans (2010) were used as references for abbreviation names of rock-forming minerals.

Scanning electron microscopy images were obtained using a Hitachi 3030TM Plus microscope operating at 15 kV in low vacuum mode and FEI Quanta 400 equipment using backscattering detectors and operating at 20 kV. Fragments were sputter-coated with silver for 250 s using a Bal-Tec SCD 005 sputter coater at 30 mA. Compositional maps were produced using energy dispersive spectrometry (EDS). Two polished sections (137.50 and 155.00) were produced to study clay mineral formation processes in the lower Codó Formation.

Whole lithogeochemical analyses were performed in bulk samples from the 1-UN-32-PI core by Act Labs (Codes 4LITHORES (11+) QOP WRA/QOP WRA 4B2 - Major and trace elements fusion ICP-OES/ICPMS and 8-Li (Sodium Peroxide Fusion) - QOP Sodium Peroxide (Sodium Peroxide Fusion) (certificate of analysis is in the Supplementary files)). These samples were also submitted to a dry ashing process at 485 °C for 24 h before analysis because of the high organic matter contents.

Lithogeochemical analyses by X-ray fluorescence spectrometry (major elements) were carried out in bulk samples from the outcrops in an Axios PANanalytical mAX spectrometer by the Center for Mineral Technology in Brazil. Samples were prepared in a BENEOX press with 30 mm of mold, with a pressure of 20 tons for 30 s, and boric acid (0.5 g/g) as the binding agent. Trace elements were not determined for outcrop samples.

A Pearson correlation matrix was constructed for the core samples (Supplementary Table S5). Samples must be carbonate-free to apply the A–CN–K (Al–(Ca + Na)–K) ternary graph as a tool to evaluate paleoweathering settings (Chemical Index of Alteration – CIA; Nesbitt and Young, 1984). Because of this, chemical contents associated with carbonates were removed from major elements before calculation (Supplementary Table S2). Due to possible weathering signatures, the outcrop samples were not used in the Pearson correlation matrix or the CIA analyses.

4. Results

4.1. Mineralogy

The diagnostic reflections used to determine each mineral are reported in Table 2. Representative diffractograms and quantitative mineralogical data are reported in Figs. 4 and 5 and in Tables 3 and 4, respectively. Saponite was identified as the species of trioctahedral smectite using the method by Christidis and Koutsopoulou (2013) and was identified at depths deeper than 137.50 m in the core and in samples from the Imperatriz outcrop, while montmorillonite was identified

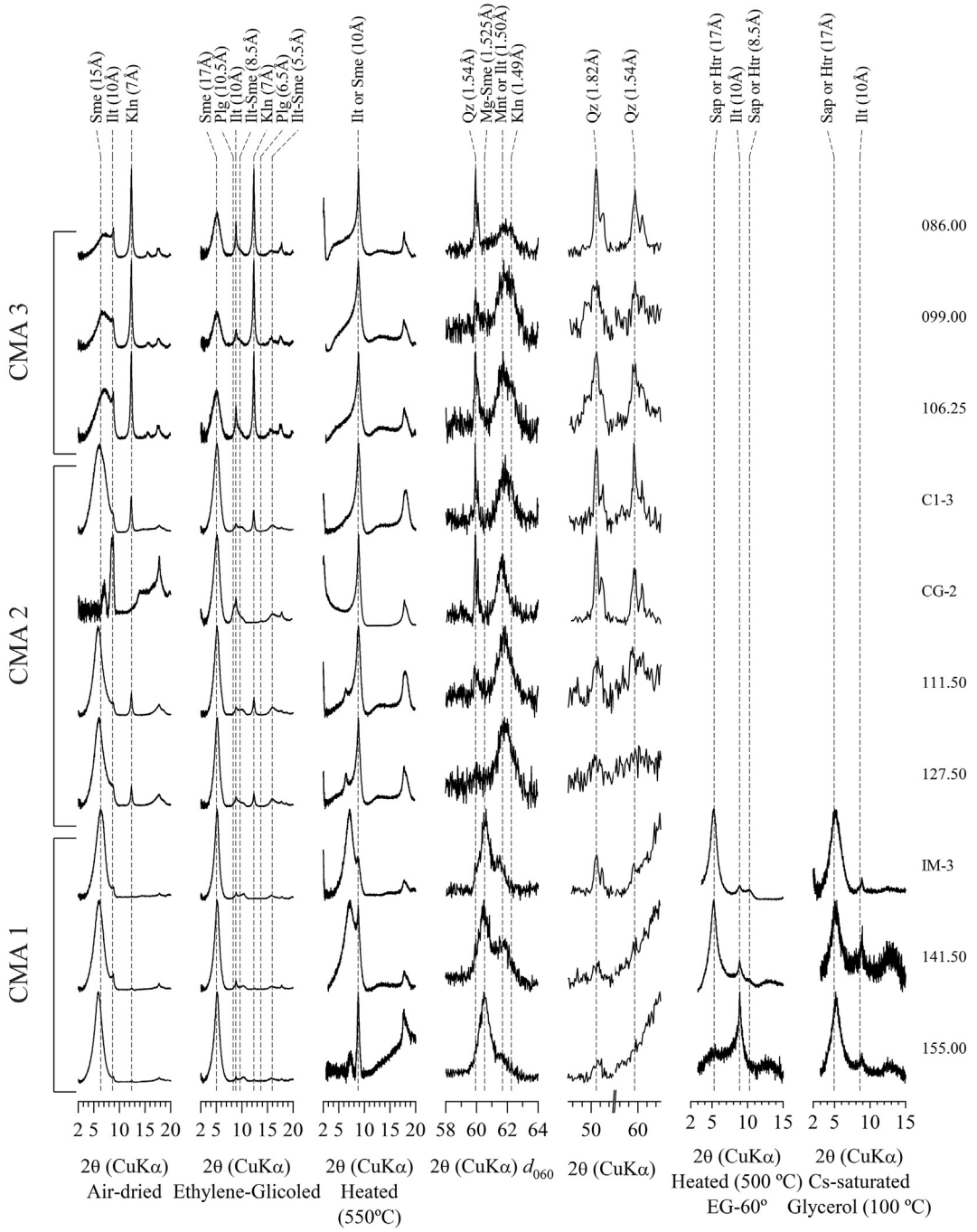

Fig. 4. Background-subtracted and normalized by maximum intensity representative diffractograms of clay fractions of the Codó Formation lutites. The method of Christidis and Koutsopoulou (2013) was used to determine the Mg-smectite species. Raw data are in supplementary files. Sme – smectite; Ilt – illite; Kln – kaolinite; Plg – palygorskite; Ilt-Sme – illite smectite mixed layered clay minerals; Qz – quartz; Mnt – montmorillonite; Mg-Sme – magnesium smectite; Sap – saponite; Htr – hectorite; CMA – clay mineral assemblage.

at depths shallower than 136.50 m and in samples from the Grajaú outcrops. Low lithium contents (0.02–0.03 wt%) were observed in the lithogeochemical analyses of trioctahedral-smectite-rich samples indicating the non-occurrence of hectorite (Table 5).

Using clay mineralogical data, three clay mineral assemblages were determined. Saponite and illite compose clay mineral assemblage 1, which comprises samples located deeper than 137 m in the core and from the Imperatriz outcrop. Clay mineral assemblage 2 contains kaolinite ranging from 5 to 15 % and comprises samples between 136.50 and 109.65 m in the core and from the Grajaú quarry. Clay mineral assemblage 3 is characterized by higher kaolinite contents ranging from 30 to 43 % (Supplementary Table S1).

4.2. Scanning electron microscopy

Clay mineral assemblages identified through X-ray diffractometry were texturally studied by scanning electron microscopy using representative fragment samples. Clay mineral assemblages 2 and 3 were found to be essentially composed of a mixture of montmorillonite, illite, and kaolinite, occurring as an oriented platy structure as well as grained crystals (Fig. 6A, B and C) (Keller, 1978). Palygorskite showed fibrous morphology (Fig. 6D). Saponite showed a hairy-shaped texture, indicative of authigenesis (Fig. 6E and F).

Two polished sections were produced to understand saponite's genesis better, and X-ray dispersive spectrometry was used to identify the

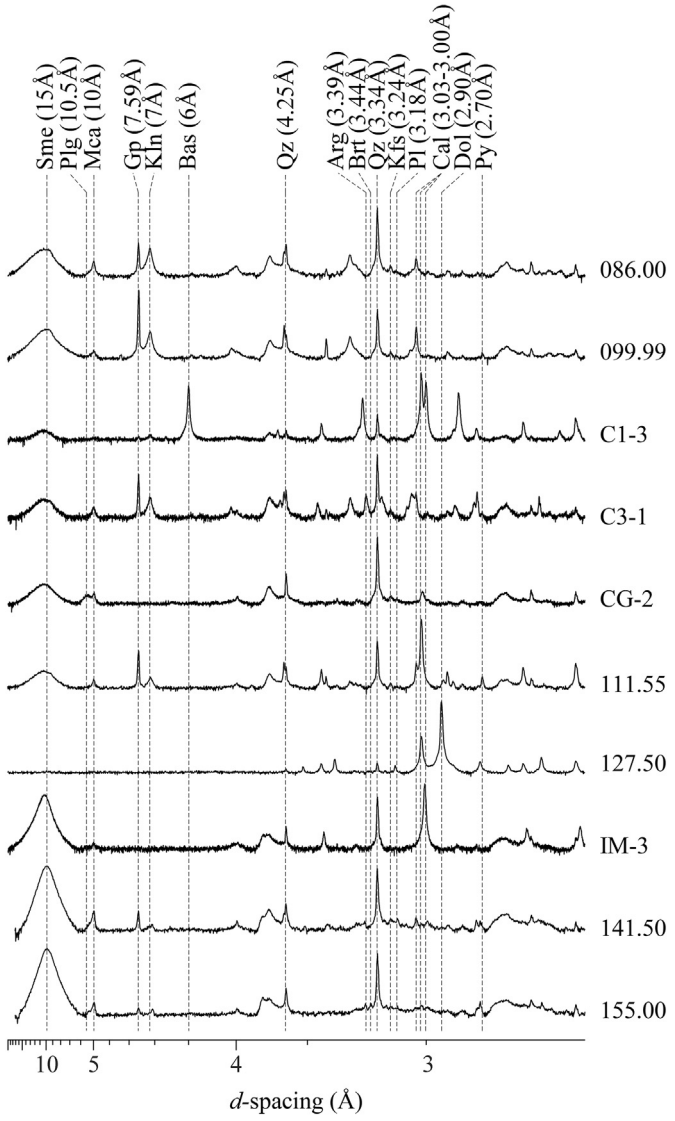

Fig. 5. Background-subtracted and normalized by maximum intensity representative diffractograms of the bulk fractions of the Codó Formation lutites. Raw data are in Supplementary files. The y-axis is in quadratic scale. Sme – smectite; Plg – palygorskite; Mca – mica; Gy – gypsum; Kln – kaolinite; Bas – bassanite; Qz – quartz; Arg – aragonite; Kfs – K-feldspar; Pl – plagioclase; Cal – calcite; Dol – dolomite; Py – pyrite.

mineral phases (Fig. 7). A matrix of saponite and minor illite contents associated with larger crystals of altered detrital clay minerals was identified. Smaller pyrite crystals occurred in the inner part of these larger crystals, whereas gypsum appeared in their central parts.

4.3. Lithogeochemistry

4.3.1. Major elements

Major elements (Table 4) were compared to the bulk mineralogy results using a Pearson correlation matrix (Supplementary Table S5). SiO_2 showed a negative correlation with dolomite. Al_2O_3 and Fe_2O_3 positively correlated with kaolinite, montmorillonite, mica and feldspars. MgO had a positive correlation with saponite and negative correlations with montmorillonite, kaolinite, gypsum, K-feldspar and plagioclase. CaO and calcite are positively correlated and K_2O and TiO_2 had positive correlations with mica and feldspars but also with montmorillonite in the case of TiO_2. Dolomite and LOI showed a positive correlation.

Table 3
Quantitative clay mineral analysis (wt%) of representative clay-sized fractions of the Codó Formation. See Supplementary Table S1 for complete data and more details.

Sample	Saponite	Montmorillonite	Palygorskite	Illite	Kaolinite	Total
C1-3	0	71	0	14	16	100
CG-2	0	55	20	24	0	100
IM-3	87	0	0	13	0	100
086.00	0	37	0	30	33	100
092.00	0	42	0	28	30	100
099.00	0	36	0	27	37	100
106.25	0	40	0	30	30	100
111.55	0	72	0	17	11	100
127.50	0	70	0	20	10	100
134.50	0	45	0	45	10	100
140.50	84	0	0	13	3	100
141.50	79	0	0	17	4	100
149.00	82	0	0	13	5	100
150.00	83	0	0	12	5	100
151.00	81	0	0	14	4	100
155.00	85	0	0	11	4	100

4.3.2. Trace elements

4.3.2.1. Large ion lithophile elements (Ba, Cs, Sr, and Rb). Trace elements are reported in Table 5. Barium and strontium did not present any correlation with the major elements and mineralogy, had higher correlation values with carbonates than silicates (Supplementary Table S5), and had similar values in comparison with those observed in the Post-Archean Australian Shale (PAAS) (Fig. 8) (McLennan, 2001; Taylor and McLennan, 1985).

Rubidium and cesium presented positive correlations with Al_2O_3, Fe_2O_3, K_2O, and TiO_2 and negative ones with LOI and CaO, being inherent from silicate minerals (e.g., feldspar or clay minerals) (Supplementary Table S5). These elements are generally depleted in comparison to PAAS, possibly due to the dilution effect subordinated to the presence of carbonate minerals (e.g., calcite, dolomite and aragonite) (Fig. 8 and Supplementary Table S5) (Tobia and Mustafa, 2016).

4.3.2.2. High-field-strength elements (Th, U, Y, Zr, Nb and Hf). All high-field-strength elements except uranium had positive correlations with oxides and were associated with silicate phases. In addition, uranium positively correlated with P_2O_5 and was probably associated with phosphate phases (Supplementary Table S5). All high-field-strength elements except uranium presented values close to those found for the PAAS (Fig. 8 and Supplementary Table S5) while uranium was enriched.

4.3.2.3. Transition trace elements (Sc, V, Cr, Co, Ni, Cu and Zn). All transition trace elements except copper and zinc had positive correlations with oxides and were associated with silicate phases, with these elements presenting values close to those found for PAAS. However, samples in the alkaline hypersaline lacustrine facies succession presented substantial positive anomalies of copper and zinc, these being values almost 40 times superior to PAAS (Table 5).

4.3.2.4. Rare earth elements. Rare earth elements (REEs) are reported in Table 6 and showed positive correlations with Al_2O_3, Fe_2O_3, TiO_2, and K_2O, associated mostly with silicate minerals (e.g., feldspar or clay minerals) (Supplementary Table S5).

5. Discussion

5.1. Origin of the clay mineral assemblages

Clay mineral assemblages 2 and 3 were understood as detrital given the lack of textures indicative of authigenesis. Palygorskite was restricted to two samples from outcrops and may theoretically have been formed by authigenesis or pedogenesis (Singer, 1979, 1984b;

Table 4
Quantitative mineral analysis (wt%) and major elements of representative bulk samples from the Codó Formation. See Supplementary Table S2 for complete data and more details.

	155.00	151.00	150.00	149.00	141.50	134.50	127.50	111.55	106.25	099.00	092.00	086.00	IM-3	CG-2	C3-1	C1-3
Mineralogy																
Saponite	87	78	78	83	81	0	0	0	0	0	0	0	66	0	0	0
Montmorillonite	0	0	0	0	0	13	0	14	24	22	21	23	0	52	21	9
Gypsum	0	1	1	0	1	7	1	11	17	15	11	6	0	0	10	1
Palygorskite	0	0	0	0	0	0	0	0	0	0	0	0	0	9	0	0
Mica	3	2	2	3	7	10	0	8	9	11	15	15	4	11	16	2
Kaolinite	0	0	0	0	0	6	0	9	22	27	26	24	0	0	23	10
Bassanite	0	0	0	0	0	0	0	0	0	0	0	0	0	0	0	59
Barite	0	0	0	0	0	0	0	0	0	0	0	0	0	0	8	0
Aragonite	1	10	5	2	0	0	0	0	0	0	0	0	0	0	0	0
Quartz	8	7	7	8	7	24	1	10	13	11	12	17	7	19	14	3
K-feldspar	0	2	2	2	3	8	0	4	8	8	9	9	0	6	0	0
Plagioclase	0	0	0	0	0	7	0	2	6	5	5	5	0	0	0	0
Calcite	0	1	1	0	0	1	18	41	1	1	1	1	23	3	0	16
Dolomite	0	0	4	0	0	23	81	1	0	0	0	0	0	0	0	0
Pyrite	0	0	1	0	1	0	0	0	1	0	1	1	0	0	7	0
Total	100	100	100	100	100	100	100	100	100	100	100	100	100	100	100	100
Chemical assay (XRF)																
SiO_2	52.05	48.11	46.55	53.27	53.75	49.12	1.06	34.72	51.31	51.37	53.50	56.45	34.50	54.50	37.60	12.50
Al_2O_3	8.56	4.51	3.92	5.54	12.78	11.51	0.27	11.15	19.33	22.67	22.87	20.79	5.30	13.80	15.90	4.60
Fe_2O_3	5.70	4.10	3.66	3.88	6.13	4.91	0.77	5.06	8.42	8.72	8.57	8.14	2.10	4.70	6.50	1.20
MnO	0.06	0.09	0.13	0.07	0.09	0.22	0.28	0.32	0.04	0.05	0.06	0.05	0.15	0.05	0.05	0.05
MgO	18.26	17.83	18.21	18.47	13.63	8.38	15.01	2.70	2.64	2.65	2.68	2.39	14.90	4.20	2.70	1.00
CaO	2.89	8.73	9.76	4.71	1.89	8.18	37.55	24.58	2.65	1.68	1.61	1.30	10.80	2.50	0.85	30.90
Na_2O	0.64	0.48	0.44	0.60	0.79	0.71	0.08	0.13	0.21	0.14	0.19	0.19	0.18	0.21	0.14	0.05
K_2O	1.48	0.57	0.46	0.74	2.62	2.34	0.03	1.68	2.43	2.36	2.62	2.65	0.65	2.10	1.80	0.42
TiO_2	0.43	0.20	0.18	0.26	0.65	0.70	0.01	0.49	0.66	0.80	0.74	1.11	0.23	0.59	0.48	0.13
P_2O_5	0.38	0.64	0.56	0.74	0.27	0.16	0.07	0.15	0.79	0.12	0.21	0.13	0.18	0.24	0.11	0.05
LOI	9.48	14.91	15.10	11.40	7.98	12.54	42.93	17.61	10.11	8.78	7.10	7.33	30.47	17.05	30.30	49.00
Total	99.93	100.17	98.97	99.68	100.58	98.76	98.06	98.59	98.59	99.35	100.14	100.53	99.46	99.94	96.43	99.90

Singer and Norrish, 1974). This clay mineral was interpreted as originating from pedogenic processes because of the intense weathering conditions observed in the quarry where the samples were collected and because this clay mineral was not observed in any sample collected from the 1-PI-UN-32 core.

Mg-clay minerals can be classified as Al-bearing Mg-clay minerals, which include saponite, hectorite and palygorskite, or as Al-free Mg-clay minerals, which comprise stevensite, talc, kerolite and sepiolite (Pozo and Calvo, 2018; Galán and Pozo, 2011; Guggenheim et al., 2006; Weaver, 1984). The source of structural aluminum in Mg-clay minerals is associated with the transformation of detrital Al-bearing clay minerals, such as montmorillonite, kaolinite or illite, into Al-bearing Mg-clay minerals (Trauth, 1977; Weaver and Beck, 1977). Mg-clay minerals are formed in specific physicochemical conditions involving high-pH water (~8–10) and high Mg^{2+} and $SiO_{2(aq)}$ concentrations (Chase et al., 2021; Tutolo and Tosca, 2018; Tosca, 2015; Tosca and Masterson, 2014; Birsoy, 2002).

Three sedimentological processes lead to the precipitation of authigenic Mg-clay minerals in sedimentary environments (Pozo and Calvo, 2018; Singer, 1979, 1984b; Singer and Norrish, 1974). The neoformation is a syngenetic process involving direct precipitation of Al-free Mg-clay minerals in the sediment–water interface. Transformation is an eodiagenetic process where detrital clay minerals such as montmorillonite are transformed into Al-bearing Mg-clay minerals (Deocampo, 2015; Hover and Ashley, 2003; Weaver and Beck, 1977; Trauth, 1977). Lastly, neoformation by addition is a process similar to transformation but occurs syngenetically (Calvo and Pozo, 2015; Galán and Pozo, 2011; Pozo and Calvo, 2018).

Lithogeochemical constraints in trace elements, mainly REEs, are observed in lutites composed of authigenic clay minerals formed by neoformation, transformation and neoformation by addition (Wilson and Pittman, 1977). Trace elements are less abundant in authigenic clay minerals formed by neoformation than in detrital clay minerals, which results from lesser concentrations of trace elements in the water table. These elements tend to be more abundant in lutites composed of authigenic clay minerals produced by transformation or neoformation by addition since the skeletal structure of detrital clay minerals is used in their formation processes. Texture differences can also be observed between clay minerals formed by neoformation or transformation and neoformation by addition (Galán and Pozo, 2011). Clay minerals formed by neoformation show clearly separated particles, while those formed by transformation or neoformation by addition present a dirty aspect.

Clay mineral assemblage 1 comprises authigenic saponite and detrital illite and represents a predominantly authigenic clay mineral assemblage in the lower Codó Formation. The genetic interpretation of authigenic saponite was mainly based on diagnostic textures observed by scanning electron microscopy (Figs. 6 and 7). Detrital clay minerals turn into saponite in an ongoing process by transformation or neoformation by addition in response to alkaline pH values (~8–10) and hypersaline conditions. This interpretation is corroborated by the lesser trace element abundances in the alkaline lake samples than in the lagoon samples and because of the dirty aspect of the samples observed by scanning electron microscopy.

5.2. An alkaline hypersaline lake in the lower Codó Formation

Alkaline hypersaline lakes are a special type of closed lacustrine depositional systems with high-pH water (~8–10) and salinity values higher than seawater (Javor, 2012). These environments are generally formed in arid climate settings and are globally known for having high algal organic matter contents, which produce remarkable source rocks in oil systems. These conditions can be produced in response to high carbonate and bicarbonate concentrations, these being important nutrients for photosynthesis. These components generally originate from carbonaceous or mafic-ultramafic source areas (Cohen, 2003).

Some of the most important ancient alkaline hypersaline paleolakes in the world are the Barremian–Aptian Atafona and Coqueiros formations (Campos Basin, Brazil) (Winter et al., 2007) and the Barremian–Aptian Piçarras and Barra Velha formations (Santos Basin, Brazil)

Table 5
Trace elements (ppm) of representative bulk samples from the Codó Formation. See Supplementary Table S3 for complete data and more details.

	155.00	151.00	150.00	149.00	141.50	134.50	127.50	111.55	106.25	099.00	092.00	086.00
Elements												
Sc	10.00	5.00	4.00	6.00	14.00	13.00	0.50	11.00	20.00	23.00	23.00	20.00
Be	2.00	1.00	0.50	1.00	2.00	2.00	0.50	2.00	3.00	4.00	3.00	4.00
V	122.00	178.00	179.00	215.00	124.00	121.00	44.00	87.00	130.00	139.00	156.00	148.00
Cr	50.00	30.00	20.00	40.00	80.00	70.00	10.00	50.00	90.00	110.00	110.00	100.00
Co	10.00	49.00	39.00	22.00	18.00	31.00	4.00	19.00	22.00	22.00	23.00	21.00
Ni	30.00	50.00	40.00	30.00	50.00	70.00	10.00	40.00	70.00	70.00	70.00	70.00
Cu	20.00	500.00	360.00	310.00	70.00	50.00	0.50	90.00	60.00	60.00	70.00	50.00
Zn	50.00	3840.00	3460.00	1210.00	60.00	50.00	15.00	40.00	70.00	90.00	90.00	180.00
Ga	13.00	8.00	7.00	8.00	18.00	16.00	1.00	14.00	27.00	29.00	28.00	27.00
Ge	1.00	0.25	0.25	0.25	0.25	0.25	0.25	0.25	1.20	1.30	1.60	0.25
As	5.00	40.00	40.00	16.00	2.50	8.00	2.50	2.50	2.50	2.50	2.50	2.50
Rb	66.00	28.00	22.00	35.00	97.00	90.00	1.00	69.00	133.00	137.00	143.00	142.00
K (%)	1.23	0.47	0.38	0.61	2.17	1.94	0.02	1.39	2.02	1.96	2.17	2.20
K	12,286.11	4731.81	3818.66	6143.05	21,749.73	19,425.33	249.04	13,946.39	20,172.46	19,591.36	21,749.73	21,998.78
Sr	521.00	1152.00	951.00	582.00	309.00	170.00	1481.00	152.00	361.00	187.00	178.00	143.00
Y	16.60	15.40	13.20	15.30	19.40	21.60	3.20	19.70	58.70	26.20	25.60	28.20
Zr	62.00	34.00	32.00	42.00	90.00	167.00	5.00	101.00	122.00	138.00	126.00	170.00
Nb	6.10	3.60	2.90	4.20	12.00	12.60	< 0.2	11.00	18.00	22.20	17.70	23.10
Mo	2.00	22.00	21.00	10.00	8.00	3.00	1.00	4.00	4.00	1.00	2.00	< 2
Ag	0.25	1.00	0.80	0.25	0.25	0.25	0.25	0.25	0.25	0.25	0.25	0.25
In	0.05	0.30	0.20	0.10	0.10	0.05	0.05	0.05	0.10	0.10	0.10	0.10
Sn	2.00	1.00	1.00	1.00	2.00	2.00	0.50	1.00	3.00	3.00	3.00	3.00
Sb	0.30	1.70	1.80	0.90	0.20	0.30	< 0.2	< 0.2	0.40	0.50	0.30	1.90
Cs	5.80	2.60	2.20	3.40	9.80	6.90	0.10	3.50	6.90	7.60	7.20	5.80
Ba	183.00	88.00	80.00	115.00	269.00	274.00	3052.00	178.00	867.00	277.00	589.00	372.00
La	25.50	19.10	14.30	17.50	33.90	31.00	4.17	34.80	77.30	58.50	53.00	58.80
Ce	55.40	36.30	27.70	36.40	71.20	62.30	6.64	67.00	180.00	104.00	102.00	103.00
Pr	6.10	4.01	3.07	4.18	7.98	7.31	0.67	7.60	21.90	12.10	11.50	11.40
Nd	23.90	14.50	11.40	15.50	30.40	27.70	2.16	28.10	88.80	43.30	43.00	41.10
Sm	4.59	2.76	2.10	2.94	5.67	5.45	0.43	5.08	19.20	7.71	7.92	7.03
Eu	0.89	0.60	0.47	0.60	1.16	1.13	0.16	1.11	3.72	1.51	1.55	1.44
Gd	3.55	2.37	1.87	2.40	4.36	4.19	0.42	4.16	15.90	5.61	5.78	5.61
Tb	0.55	0.39	0.30	0.39	0.66	0.66	0.07	0.62	2.43	0.88	0.89	0.84
Dy	3.17	2.31	1.84	2.37	3.77	4.13	0.37	3.49	12.70	5.16	5.06	4.96
Ho	0.62	0.46	0.39	0.45	0.72	0.74	0.08	0.67	2.20	0.98	0.95	0.96
Er	1.74	1.36	1.15	1.30	2.02	2.27	0.27	1.83	5.24	2.82	2.67	2.85
Tm	0.25	0.19	0.17	0.18	0.28	0.32	0.04	0.26	0.65	0.41	0.39	0.40
Yb	1.52	1.16	1.00	1.12	1.89	2.11	0.22	1.57	3.66	2.72	2.48	2.74
Lu	0.23	0.17	0.15	0.16	0.27	0.32	0.03	0.25	0.54	0.43	0.39	0.44
Hf	1.80	0.80	0.80	1.10	2.30	3.80	0.05	2.30	3.10	3.50	3.10	3.90
Ta	0.49	0.30	0.23	0.33	0.89	3.84	0.05	0.71	1.10	1.31	1.06	1.41
W	3.50	0.25	0.25	0.25	5.90	34.90	41.00	0.70	7.80	2.50	2.80	4.20
Tl	0.45	1.37	0.94	0.56	0.38	0.63	< 0.05	0.73	0.82	0.92	0.76	0.47
Pb	29.00	518.00	516.00	132.00	18.00	17.00	6.00	35.00	26.00	35.00	27.00	61.00
Bi	0.05	0.80	0.40	0.30	0.30	0.05	0.05	0.05	0.10	0.20	0.20	0.50
Th	8.57	4.33	3.43	4.80	10.60	9.78	0.12	9.04	16.20	18.80	15.20	18.30
U	8.13	11.80	11.60	12.40	6.24	4.03	0.54	2.42	6.30	4.82	3.26	3.66
Li	0.02	0.03	0.03	0.03	0.02							
Rb/K	0.0054	0.0059	0.0058	0.0057	0.0045	0.0046	0.0040	0.0049	0.0066	0.0070	0.0066	0.0065
La/Th	2.98	4.41	4.17	3.65	3.20	3.17	34.75	3.85	4.77	3.11	3.49	3.21
Th/Sc	0.86	0.87	0.86	0.80	0.76	0.75	0.24	0.82	0.81	0.82	0.66	0.92
Th/Co	0.86	0.09	0.09	0.22	0.59	0.32	0.03	0.48	0.74	0.85	0.66	0.87
Th/Cr	0.16	0.39	0.58	0.31	0.08	0.06	0.05	0.05	0.07	0.04	0.03	0.04
Zr/Sc	6.20	6.80	8.00	7.00	6.43	12.85	10.00	9.18	6.10	6.00	5.48	8.50
La/Sc	2.55	3.82	3.58	2.92	2.42	2.38	8.34	3.16	3.87	2.54	2.30	2.94
U/Th	0.95	2.73	3.38	2.58	0.59	0.41	4.50	0.27	0.39	0.26	0.21	0.20
V/Cr	2.44	5.93	8.95	5.38	1.55	1.73	4.40	1.74	1.44	1.26	1.42	1.48
V/Ni	4.07	3.56	4.48	7.17	2.48	1.73	4.40	2.18	1.86	1.99	2.23	2.11
Cu + Zn + Pb	99.00	4858.00	4336.00	1652.00	148.00	117.00	21.50	165.00	156.00	185.00	187.00	291.00

(Moreira et al., 2007), which compose part of the Brazilian Pre-salt oil system (Carramal et al., 2022; Lima and De Ros, 2019; Rehim et al., 1986). Other units are the Barremian–Aptian formations of the Kwanza Basin in Angola (Saller et al., 2016), the Eocene Parachute Creek Member of the Green River Formation in the USA (Smith and Carroll, 2015; Dyni, 1976), and the Pleistocene Olduvai Paleolake and the Sinya Beds of the Amboseli Basin in Tanzania (Deocampo, 2015; Hover and Ashley, 2003). Some of the most important modern alkaline hypersaline lakes are the Pantanal wetlands in Brazil (Oliveira et al., 2021; Dias et al., 2020; Furquim et al., 2008; Furquim, 2007), Lake Abert in the USA (Jones and Weir, 1983), and a series of African lakes, including Ngorongoro Lake in Tanzania and Chad Lake in the Sahara Desert (Deocampo, 2004, 2005). Alkaline lakes have also been reported as possible depositional systems on Mars (Bristow et al., 2021).

Different sedimentological, paleontological, and geochemical data can be used to recognize alkaline hypersaline lakes, but identifying authigenic Mg-clay minerals is one of the most reliable diagnostic methods (Pozo and Galán, 2015; Calvo and Pozo, 2015; Darragi and Tardy, 1987). Authigenic saponite was identified in the lower Codó Formation in the interval from 155.00 to 137.00 m (Fig. 9), comprising a total of 18 m, with this segment being diagnostic of an alkaline hypersaline lake, which explains the high organic matter contents and the

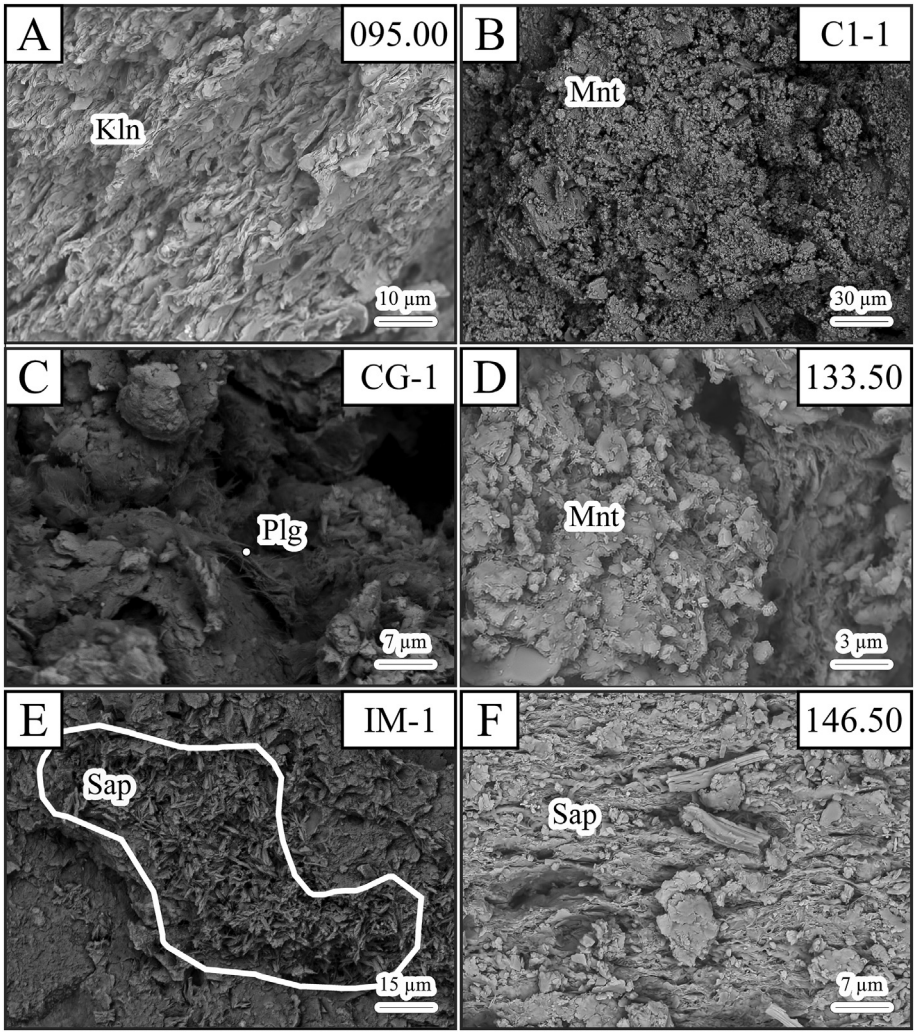

Fig. 6. Scanning electron microscopy images of representative bulk lutite samples from the Codó Formation. A, B) Crystals of detrital kaolinite, montmorillonite and illite. C) Detrital montmorillonite and fibrous palygorskite crystals originated from pedogenetic processes. D) Detrital montmorillonite, illite and kaolinite. E, F) Authigenic saponite and illite. Kln – kaolinite; Mnt – montmorillonite; Plg – palygorskite; Sap – saponite.

occurrence of biomarkers indicative of alkaline and hypersaline conditions in the Codó Formation (Bastos et al., 2022).

There are two main hypotheses for the magnesium source in the lower Codó Formation. The first is the most common reason for the formation of alkaline lakes and involves source areas composed of mafic or ultramafic rocks, generally associated with volcanically active areas (Cohen, 2003). The second is less common and is related to syngenetic hydrothermal processes, which buffer magnesium and other elements inside the lake. Lithogeochemistry can evaluate the provenance of mafic or ultramafic source areas and investigate base metal contents to check for hydrothermal influence. Anomalous base metal contents (Cu + Zn + Pb ~ 4500 ppm, Table 5), reaching values up to 40 times higher than those found in the PAAS, were observed in the depth interval between 152.00 and 149.00 m in the 1-PI-UN-32 well. Conventional sedimentological processes do not commonly generate these values, so they are likely associated with hydrothermal processes (Robb, 2020; Pirajno, 2012; Emsbo et al., 2016). This information also indicates that hydrothermal processes are the most probable source of magnesium in the Codó Formation.

Lithogeochemistry can also distinguish if the Mg-smectites were formed syngenetically in response to specific hydrochemical conditions or because of hydrothermal processes. The structure of a detrital clay mineral is partially opened when transformed into Al-bearing Mg-smectites, resulting in the reduction of REE abundance, while hydrothermal processes generally increase REE abundance, depending on its composition. The alkaline hypersaline lake samples presented lower REE values than those found in the lagoon facies succession (Table 7), which reinforces a syngenetic origin of the Al-bearing Mg-clay minerals.

5.3. Correlations with the Pre-salt depositional systems based on clay mineralogy

The Pre-salt oil system comprises part of the Lower Cretaceous interval of a set of marginal basins in the Brazilian Atlantic continental shelf, including the Campos (Winter et al., 2007) and Santos basins (Moreira et al., 2007). These rocks were deposited in a restricted nonmarine succession, including sandstones, siltstones, lutites and limestones. Talc, kerolite and stevensite are the most commonly reported authigenic clay mineral assemblages in the Atafona and Coqueiros formations (Campos Basin) and the Piçarras and Barra Velha formations (Santos Basin) (Lima and De Ros, 2019; Rehim et al., 1986).

The Codó Formation is an ancient analog of these rocks and the identification of Mg-smectite allows correlations that could help provide useful information about the general environmental evolutions that both systems experienced. The main Mg-clay mineral assemblages in siliciclastic fine-grained rocks from the Pre-salt are stevensite, talc and kerolite, while saponite is identified in the Codó Formation. The alkaline

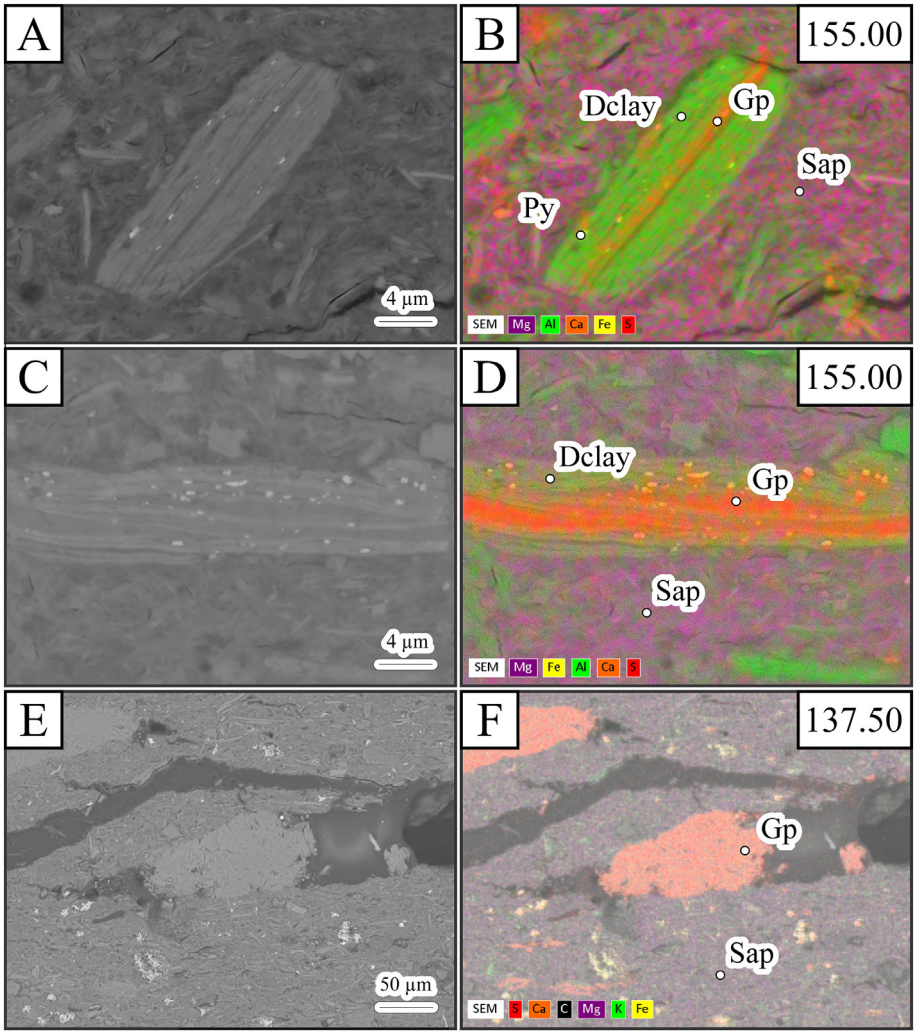

Fig. 7. Scanning electron microscopy images and compositional maps obtained from polished sections of samples located at 137.60 and 155.00 m deep. A, B) Transformation of detrital clay minerals into saponite and coprecipitation of pyrite and gypsum in initial stages. E, F) Transformation of detrital clay minerals into saponite and coprecipitation of pyrite and gypsum in intermediate stage. E, F) Transformation of detrital clay minerals into saponite and coprecipitation of pyrite and gypsum in final stages. Dclay – detrital clay mineral; Gp – gypsum; Sap – saponite; Py – pyrite.

pH and salinity conditions to precipitate these clay mineral assemblages are similar and were reached by both systems. Stevensite, saponite and hectorite are Mg-smectites commonly formed in high pH environments (Tutolo and Tosca, 2018; Tosca, 2015; Tosca and Masterson, 2014; Galán and Pozo, 2011).

The main difference between these clay mineral assemblages is the presence of Al^{3+} in the saponite structure, which demands a geochemical explanation for its presence. According to the model proposed by Pozo and Calvo (2018), Al^{3+} is associated with inherited Al-bearing clay minerals, such as montmorillonite, which was ubiquitously identified in the Codó Formation throughout this study and in literature (Gonçalves et al., 2006; Rossetti et al., 2001). This information indicates that the Codó Formation received a higher sediment supply than the Pre-salt lakes, where the lack of inherited Al-bearing clay minerals inhibited the formation of Al-bearing Mg-clay minerals and enabled only the formation of Al-free Mg-clay minerals.

5.4. A paleoclimate change in Northeastern Brazil during the late Aptian

Paleoclimate reconstructions, which combine paleoprecipitation and paleotemperature aspects, are essential to understand the development of depositional systems and the evolution of fauna and flora in sedimentary records (Ramstein et al., 2020; Cronin, 1999). Arid to semiarid paleoclimate settings have been described in the South American Equatorial Atlantic Margin during the Early Cretaceous based on clay mineralogical, lithological, and paleontological data (Salgado-Campos et al., 2021; Boucot et al., 2013; Hay and Floegel, 2012; Chumakov et al., 1995; Lima, 1983; Petri, 1983).

Based on the occurrence of evaporite rocks, this region was interpreted as an evaporative zone by Chumakov et al. (1995) in a Tropical–Equatorial hot arid belt, while Boucot et al. (2013) attributed an arid zone based on the same lithological data. In addition, these authors observed a humidification process in the Aptian–Albian transition based on Albian kaolin deposits in the African Equatorial Atlantic Margin counterpart (Agumanu and Enu, 1990). One of the main possible causes of this climate change is the Supercontinent Effect hypothesis, which considers that before the Gondwana breakup, which occurred from the Early Jurassic to Late Cretaceous and developed from south to north in South America (Voo, 1993), the large dimensions of the continent hindered moisture from penetrating it (Hay and Floegel, 2012; Skelton et al., 2003).

Two detrital clay mineral assemblages reflecting different climate conditions were determined through semi-quantitative clay mineral analyses in the Codó Formation (Fig. 10a). Clay mineral assemblage 2 was observed in samples located from 136.50 to 110.65 m deep, comprising mostly the sabkha facies association, with kaolinite concentrations up to

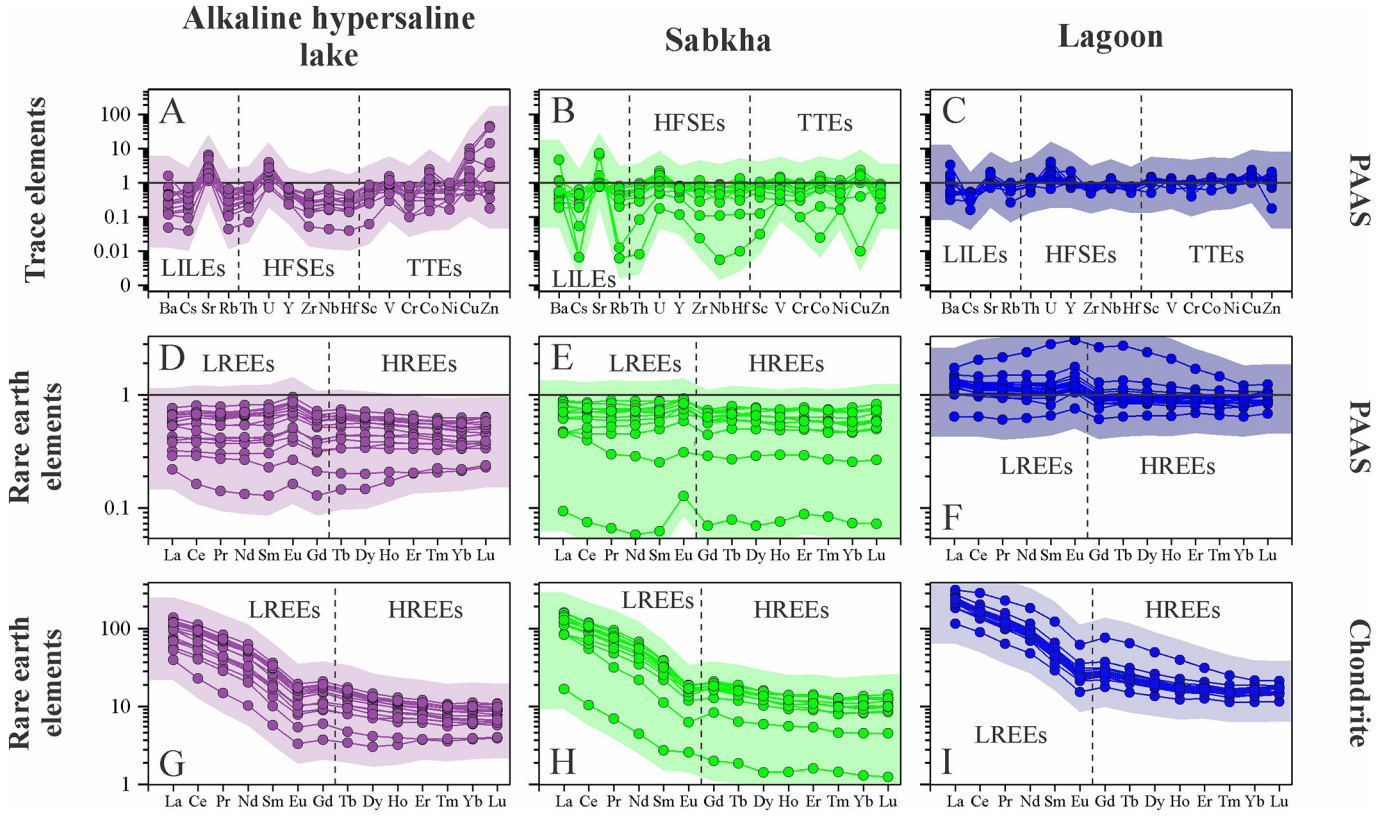

Fig. 8. Trace and rare earth element diagrams of the Codó Formation lutites normalized by the Post-Archean Australian Shale (PAAS) and by chondrite. A, B, C) PAAS-normalized trace elements (Taylor and McLennan, 1985). D, E, F) REE values normalized by PAAS (Pourmand et al., 2012). G, H, I) REE values normalized by chondrite (Pourmand et al., 2012). Large ion lithophile elements - LILE. High-field strength elements - HFSE. Transition trace elements - TTE. Light rare earth elements - LREEs. Heavy rare earth elements - HREEs.

15 %. Clay mineral assemblage 3 was identified in samples located between 108.65 and 86 m deep, comprising mostly the lagoon facies association, with kaolinite concentrations ranging from 30 to 43 % (Supplementary Table S5).

Detrital clay mineral assemblage 2 has indicated low paleoprecipitation values (<250 mm), which can be related to arid climate conditions, while detrital clay mineral assemblage 3 has indicated higher paleoprecipitation values (~400 mm) (Fig. 10a). These values revealed a

Table 6
Rare earth elements (ppm) of representative bulk samples from the Codó Formation. See Supplementary Table S4 for complete data and more details. Anomalies were calculated using Taylor and McLennan (1985).

	155.00	151.00	150.00	149.00	141.50	134.50	127.50	111.55	106.25	099.00	092.00	086.00
Elements												
La	25.50	19.10	14.30	17.50	33.90	31.00	4.17	34.80	77.30	58.50	53.00	58.80
Ce	55.40	36.30	27.70	36.40	71.20	62.30	6.64	67.00	180.00	104.00	102.00	103.00
Pr	6.10	4.01	3.07	4.18	7.98	7.31	0.67	7.60	21.90	12.10	11.50	11.40
Nd	23.90	14.50	11.40	15.50	30.40	27.70	2.16	28.10	88.80	43.30	43.00	41.10
Sm	4.59	2.76	2.10	2.94	5.67	5.45	0.43	5.08	19.20	7.71	7.92	7.03
Eu	0.89	0.60	0.47	0.60	1.16	1.13	0.16	1.11	3.72	1.51	1.55	1.44
Gd	3.55	2.37	1.87	2.40	4.36	4.19	0.42	4.16	15.90	5.61	5.78	5.61
Tb	0.55	0.39	0.30	0.39	0.66	0.66	0.07	0.62	2.43	0.88	0.89	0.84
Dy	3.17	2.31	1.84	2.37	3.77	4.13	0.37	3.49	12.70	5.16	5.06	4.96
Ho	0.62	0.46	0.39	0.45	0.72	0.74	0.08	0.67	2.20	0.98	0.95	0.96
Er	1.74	1.36	1.15	1.30	2.02	2.27	0.27	1.83	5.24	2.82	2.67	2.85
Tm	0.25	0.19	0.17	0.18	0.28	0.32	0.04	0.26	0.65	0.41	0.39	0.40
Yb	1.52	1.16	1.00	1.12	1.89	2.11	0.22	1.57	3.66	2.72	2.48	2.74
Lu	0.23	0.17	0.15	0.16	0.27	0.32	0.03	0.25	0.54	0.43	0.39	0.44
LREEs	115.49	76.67	58.57	76.52	149.15	133.76	14.07	142.58	387.20	225.61	217.42	221.33
HREEs	17.11	11.77	9.43	11.90	20.80	21.31	2.09	19.05	66.25	28.23	28.08	27.27
ΣREEs	128.01	85.68	65.90	85.48	164.28	149.62	15.73	156.55	434.25	246.13	237.58	241.57
Ce/Ce*	1.04	0.97	0.98	1.00	1.01	0.97	0.93	0.97	1.03	0.92	0.97	0.93
Pr/Pr*	1.01	1.05	1.04	1.06	1.03	1.06	1.07	1.05	1.04	1.09	1.05	1.05
Eu/Eu*	0.67	0.72	0.72	0.69	0.71	0.72	1.11	0.74	0.65	0.70	0.70	0.70
Gd/Gd*	1.18	1.14	1.16	1.15	1.15	1.12	0.92	1.16	1.23	1.13	1.14	1.18
(Gd/Yb)n	1.53	1.34	1.23	1.41	1.52	1.30	1.25	1.74	2.85	1.35	1.53	1.34
(La/Yb)n	7.66	7.52	6.53	7.13	8.19	6.71	8.66	10.12	9.64	9.82	9.76	9.80

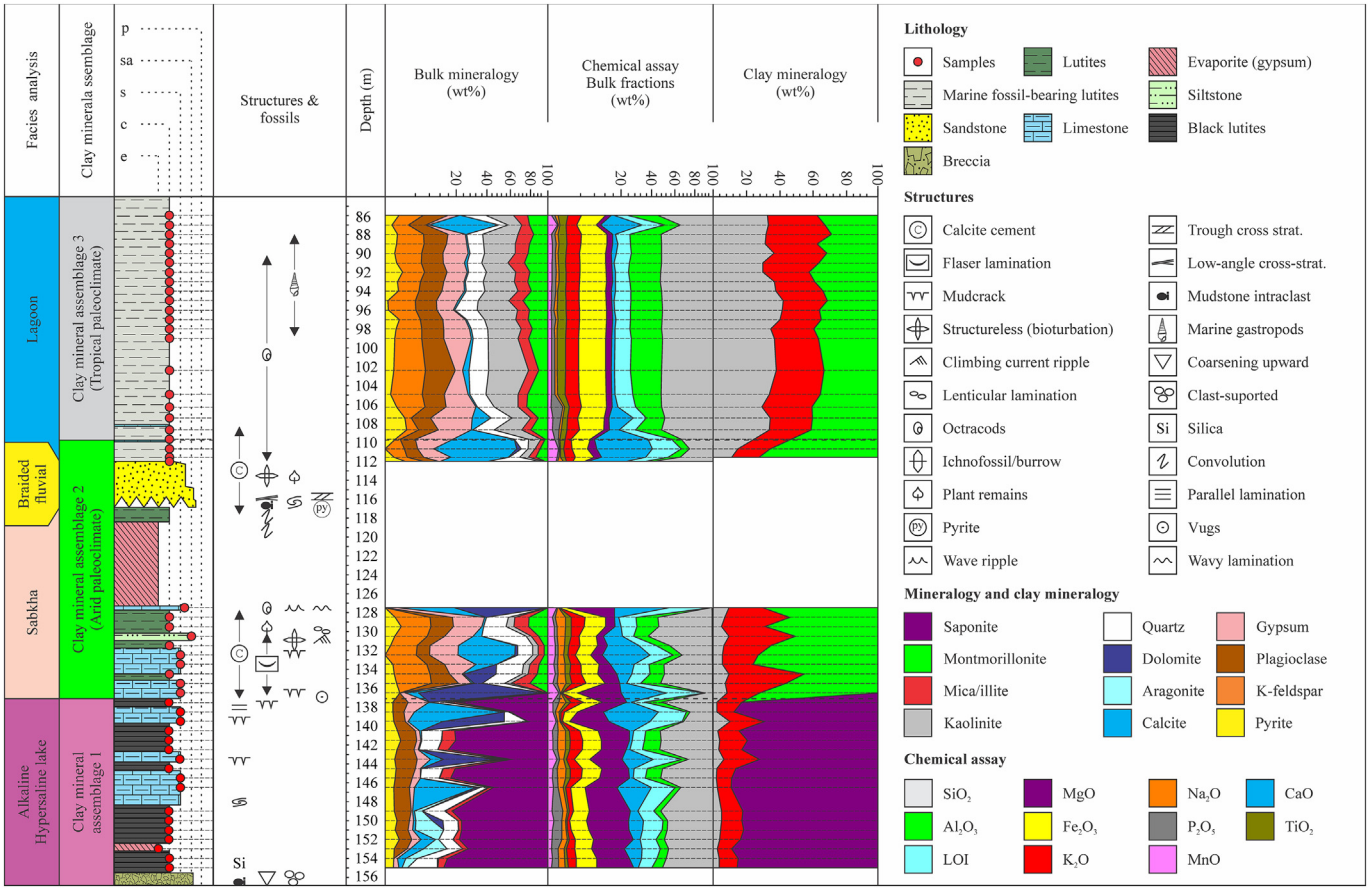

Fig. 9. Mineralogy and lithogeochemistry (major elements) profile of lutites from the Codó Formation. Lithological features and facies analysis are from Mendes (2007). The x-axes are in the bulk mineralogy and chemical assay logs on a quadratic scale. Raw data are in the Supplementary files.

humidification process and a climate change in Northeastern Brazil during the late Aptian. This interpretation is corroborated by the increasing CIA values from the sabkha samples to the lagoon samples, indicating stronger weathering conditions (Fig. 11).

The change in detrital clay mineral assemblage 3 coincides with marine fossil occurrences (i.e., dinoflagellates and gastropods) in the upper Codó Formation (Alvarenga, 2010; Mendes, 2007; Neves, 2007). These occurrences indicate that the sea played a major role in this climate change and supports the model which attributes this humidification process to the proximity between the land and sea, which was caused by the Gondwana breakup (i.e., The Supercontinent effect; Hay and Floegel, 2012).

Two paleoclimate reconstruction maps were produced, compiling new clay mineralogical data, lithologies and quantitative clay mineralogical data available in the literature (Fig. 10b and c) (see references in Table 8). In addition, an arid-tropical binary system was used (Boucot et al., 2013), using revised and updated Brazilian lithological climate indicators (Supplementary Table S6).

The first paleoclimate reconstruction is due to the late Aptian and it shows arid climate conditions in Northeastern Brazil, which is mainly evidenced by low kaolinite contents in detrital clay mineral assemblages from the lower part of the Codó Formation and in the Rio da Batateira and Santana formations (Araripe Basin, Brazil) (Salgado-Campos et al., 2021; Teles and Berthou, 1995). The second climate

Table 7
Comparisons with felsic and mafic sources and paleoenvironmental and provenance proxies using lithogeochemical ratios of the Codó Formation lutites. Numbers represent the minimum, maximum and average values, respectively.

Proxies	Alkaline hypersaline lake (n = 17)	Sabkha (n = 7)	Lagoon (n = 20)	Felsic rocks	Mafic rocks
Paleoenvironment					
Rb/K paleosalinity	0.0042–0.0059 (0.0050) Brackish water	0.0037–0.0080 (0.0048) Brackish water	0.0054–0.0074 (0.0067) Seawater	–	–
Cu + Zn + PB hydrothermal influence	75–4858 (800)	21–249 (145)	142–291 (202)	–	–
Provenance					
Th/Sc	0.66–1.02 (0.81)	0.24–0.88 (0.68)	0.66–0.96 (0.80)	0.84–20.50	0.05–0.22
Th/Co	0.09–0.88 (0.53)	0.03–2.48 (0.57)	0.27–0.98 (0.75)	0.67–19.40	0.04–1.40
Th/Cr	0.08–0.58 (0.19)	0.05–0.15 (0.08)	0.02–0.27 (0.06)	0.13–2.70	0.018–0.046
La/Sc	2.11–9.73 (3.22)	1.89–10.50 (3.59)	2.23–3.87 (2.73)	2.50–16.30	0.43–0.86
Eu/Eu*	0.63–0.76 (0.71)	0.62–1.11 (0.73)	0.65–0.77 (0.70)	0.40–0.94	0.71–0.95
LREEs	31–149 (99)	14–163 (116)	119–387 (223)	–	–
HREEs	4–21 (14)	2–22 (17)	19–66 (29)	–	–
ΣREEs	35–164 (110)	16–177 (128)	133–434 (245)	–	–

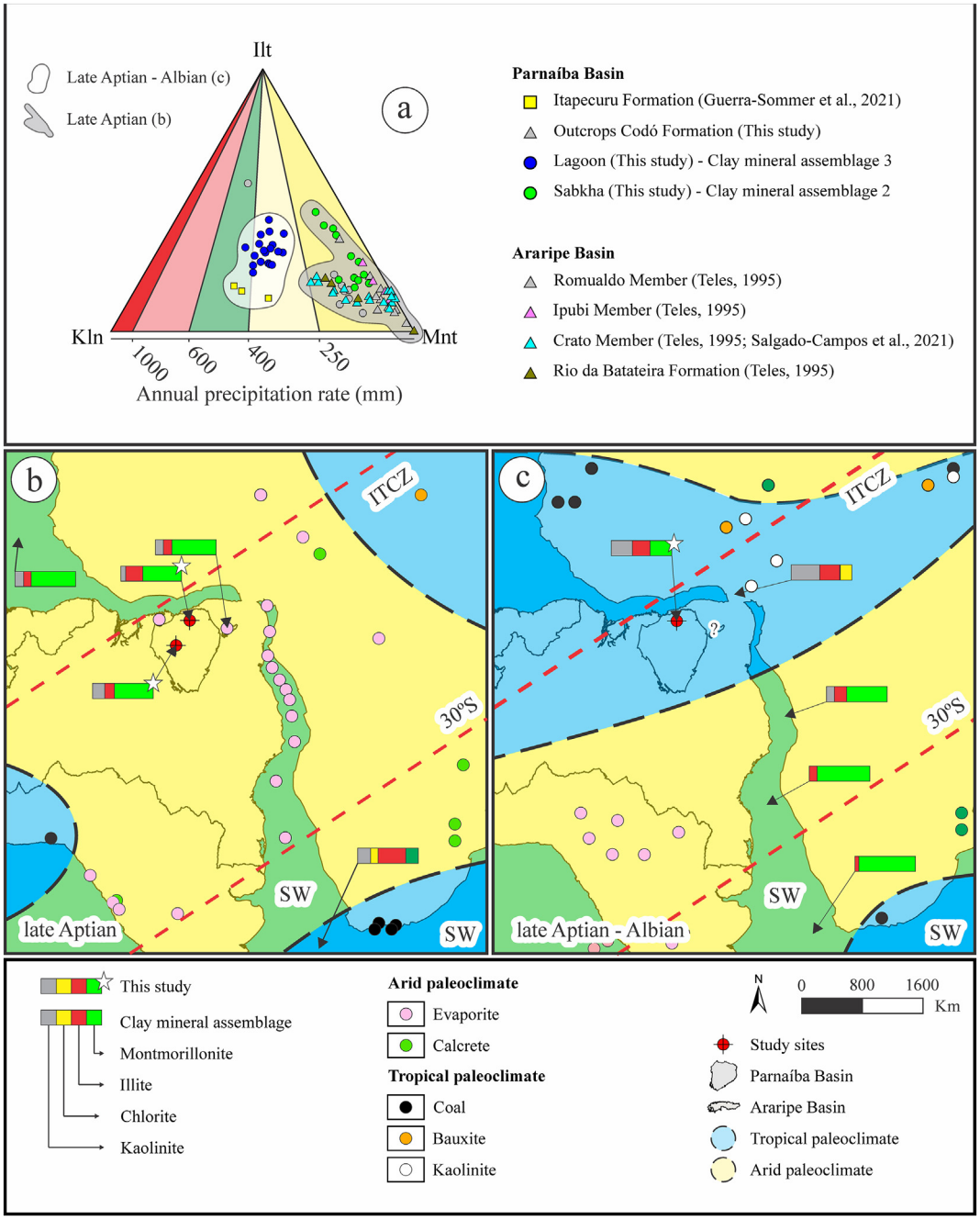

Fig. 10. Lower Cretaceous paleoclimate maps of the Equatorial Atlantic Margin based on lithological and clay mineralogical data. Raw data can be found in Supplementary Table S6. Paleogeographic maps were reconstructed to 120.8 Ma using Matos et al. (2021a) and produced using GPlate 2.3.0 software. The Barremian paleowind reconstruction of Scherer et al. (2020) was used. Intertropical Convergence Zone (ITCZ) is a convergence zone of winds near the Equator. SW – seawater. a) Ternary diagram based on the clay mineralogy used to reconstruct paleoprecipitation values (Barshad, 1966) during the late Aptian using data from the Parnaíba and Araripe basins (Guerra-Sommer et al., 2021; Salgado-Campos et al., 2021; Teles and Berthou, 1995). b) Late Aptian paleoclimate map (references in Table 8). c) Late Aptian–Albian paleoclimate map (references in Table 8).

reconstruction is also due to the late Aptian but comprises Albian data. Tropical conditions were attributed to Northeastern Brazil since higher kaolinite contents were observed in detrital clay mineral assemblages in the upper Codó Formation (herein) and the African counterpart (Agumanu and Enu, 1990). This interpretation corroborates the early onset hypothesis of the Equatorial humid belt in the equatorial Atlantic Margin proposed by Santos et al. (2022) using lithological and palynological data. This event was also recognized by Carvalho et al. (2019) in the Sergipe–Alagoas basin and by Carvalho et al. (2010) using paleontological data.

5.5. Depicting paleoenvironmental significance for the lithofacies and facies successions

Lithogeochemistry has been widely used to study sedimentary environments and evaluate depositional conditions using elemental ratios. Rubidium vs potassium is a paleosalinity proxy based on the correlative pattern among lutites formed in marine and nonmarine environments (Geiger, 2000; Visser and Young, 1990; Campbell and Williams, 1965; Campbell and Lerbekmo, 1963). Plots of the sabkha samples indicated mostly brackish water, while the plots of the lagoon samples indicated

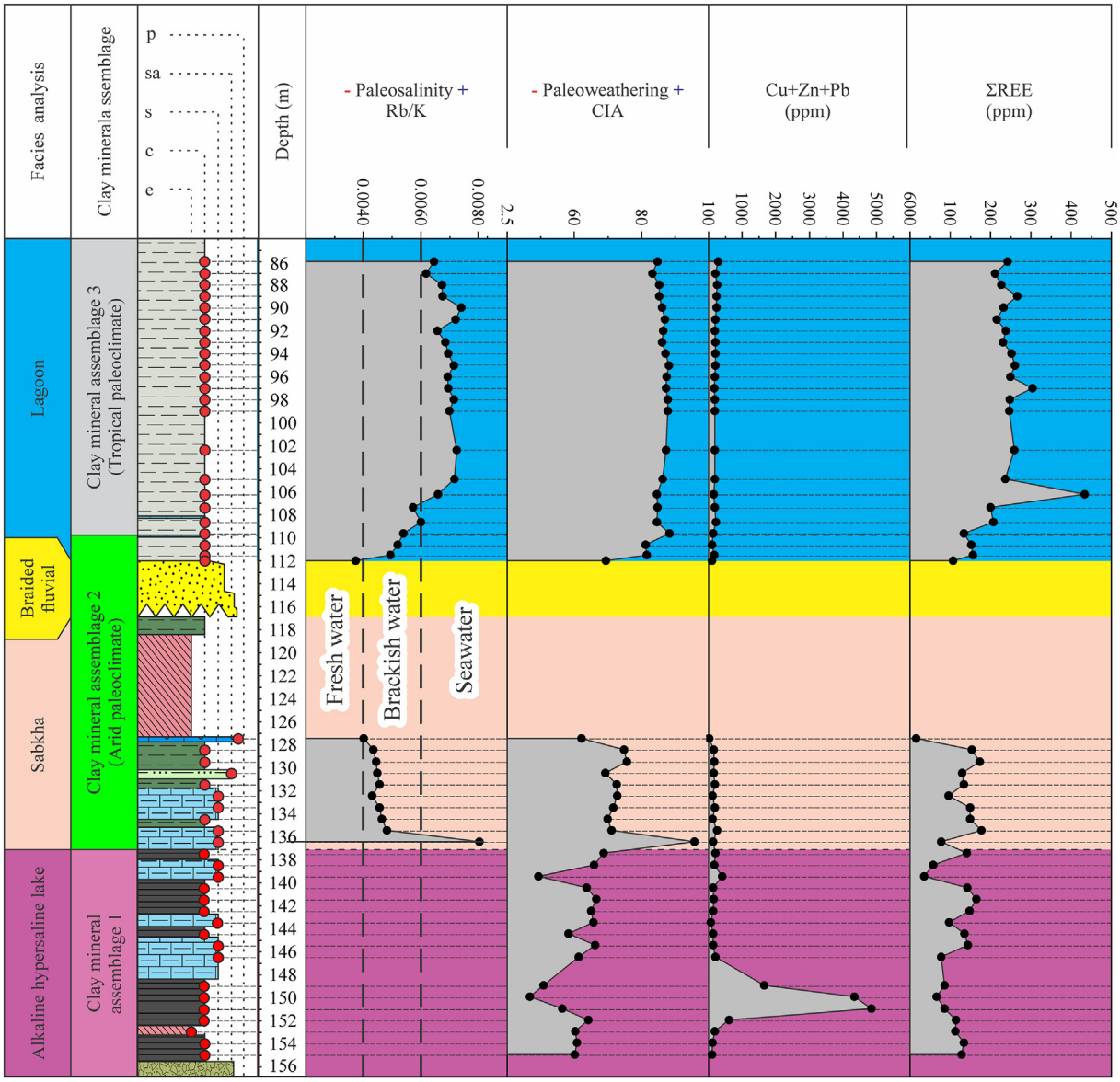

Fig. 11. Paleoenvironmental and paleoclimatic proxy profiles of the Codó Formation based on lithogeochemical data, namely paleosalinity, paleoenvironmental, paleoredox, paleoweathering, base metal contents and ΣREEs. Lithological features and facies analysis are from Mendes (2007). e – evaporite; c – clay; s – silt; sa – sand; p – pebble.

seawater conditions (Fig. 11). This interpretation is corroborated by paleontological data (Barros et al., 2022). However, this proxy cannot be used to reconstruct paleoenvironmental conditions in alkaline lakes due to trace element modifications in response to authigenic processes. The salinity of this facies succession was interpreted as hypersaline based on the occurrence of indicative biomarker data (Bastos et al., 2022).

The lithofacies and facies successions proposed by Mendes (2007) were reinterpreted in light of new mineralogical and lithogeochemical data. The bituminous lutites interlaminated with gypsum and limestone laminae (Ab), in intervals ranging from 155 to 137 m, were formed by decantation of clay-sized particles from suspension followed by clay authigenesis. This process took place in the substrate and at the sediment–water interface and occurred associated with the precipitation of carbonate (i.e., calcite or dolomite) and sulfate (gypsum) minerals. This lithofacies was formed in a subaqueous environment with episodes of subaerial exposure due to mudcracks. The clay authigenesis process involved transformation or neoformation by adding detrital clays (montmorillonite, kaolinite or illite) into saponite in response to hypersaline and alkaline conditions.

This lithofacies composes the hypersaline lake proposed by Mendes (2007), which was reinterpreted as a magnesium-sulfate-rich shallow alkaline hypersaline lake with shallowing upward cycles. The higher contents of calcite or dolomite coincided with mudcracks and were associated with periods of subaerial exposure and lowstand phases, while the highest mud content was correlated with highstand phases, indicating a higher siliciclastic input rate.

A sudden salinity-increasing event was observed at the interface between the alkaline hypersaline lake and sabkha using lithogeochemical data (e.g., Rb/K; Fig. 11), which can be interpreted as the first relevant marine ingression episode in the Codó Formation. This episode changed the lake's pH from alkaline to acid, inhibiting the formation of Mg-smectites and changing its hydrochemical conditions.

The bituminous lutites interlaminated with gypsum and limestone layers (Ab), in the interval from 137 to 110 m, did not contain Al-bearing Mg-clay minerals. These mixed carbonate–siliciclastic lithologies were deposited under concomitant decantation of clay-sized particles from suspension and coprecipitation of carbonate (calcite or dolomite) and sulfate (gypsum) minerals in a subaqueous saline environment.

Table 8
Compilation of references used in the construction of paleoclimate maps in Fig. 10b and c. See more details in Supplementary Table S6.

Late Aptian paleoclimate map (a)			
Assine (2007)	França et al. (2007)	Martill (1993)	Rodovalho et al. (2007)
Bell and Padian (1995)	Germann et al. (1990)	Matos et al. (2021b)	Rona (1982)
Bell (1989)	Góes and Feijó (1994)	McLachlan and McMillan (1976)	Rossetti and Góes (2000)
Benavides (1962)	Gontijo et al. (2007)	McMillan et al. (1997)	Salgado-Campos et al. (2021)
Bueno et al. (2007)	Graddi et al. (2007)	Moody and Sutcliffe (1991)	Santos et al. (1994)
Caixeta et al. (2007)	Greigert (1966)	Moody (1997)	Schmidt et al. (1995)
Campos Neto et al. (2007)	Grimaldi et al. (1990)	Moreira et al. (2007)	Suarez and Bell (1987)
Congleton (1990)	Harris et al. (2000)	Netto et al. (1994)	Thiry and Jacquin (1993)
Córdoba et al. (2007)	Heimhofer et al. (2010)	Pereira and Feijó (1994)	Vanderstappen and Verbeek (1959)
Coward et al. (1999)	Joulia (1959)	Ponte and Appi (1990)	Vieira et al. (1994)
De Ruiter (1979)	Joulia et al. (1958)	Rangel et al. (1994)	Winter et al. (2007)
Dias et al. (1994)	Katz and Mello (2000)	Rangel et al. (2007)	Wipki et al. (1993)
Dingle et al. (1983)	Lima et al. (1994)	Riccardi (1988)	Zalán and Romeiro-Silva (2007)
Feijó (1994)			

Late Aptian–Albian paleoclimate map (b)			
Agumanu and Enu (1990)	Germann et al. (1990)	McMillan et al. (1997)	Weaver et al. (1990)
Benavides (1962)	Hartley et al. (1992)	Moody and Sutcliffe (1991)	
Brownfield and Weaver (1992)	Jones (1948)	Riccardi (1988)	
Enu (1980)	McLaughlin Jr (1972)	Salgado et al. (1997)	

This lithofacies composed the biggest part of the sabkha interpreted by Mendes (2007), who considered the upper limit of this facies succession to be at the bottom of the sandstone bedset (~117 m), where there was a probable unconformity. This facies succession was reinterpreted as a marine-influenced sulfate-rich acid sabkha due to the occurrence of the gypsum bed and the absence of Al-bearing Mg-clay minerals, which indicate lower pH values.

The fossiliferous lutites with ostracods and marine gastropods (Af) ranged from 110 to 86 m and compose the marine-dominated phase of the lake, according to Mendes (2007), mainly because of the occurrence of marine gastropods. Seawater conditions were inferred using lithogeochemical data and corroborated the marine character of this succession.

5.6. Provenance reconstructions using lithogeochemistry

Elemental ratios are also applied to obtain compositional and tectonic information on source rocks. An incompatible element fills the numerator and a compatible element fills the denominator (Taylor and McLennan, 1985). Therefore, the more evolved and felsic the source rock, the higher the ratio. Lithogeochemical ratios and europium anomalies indicated provenance mostly from post-Archean intermediate rocks and a common compositional and source area to the studied section (Table 7).

Most of the samples plotted in the acid or intermediate compositional field in the potassium vs rubidium graph (Fig. 12A) (Floyd and Leveridge, 1987). However, samples from the alkaline hypersaline lake interval plotted in the basic compositional field. Samples plotted in the felsic volcanic to granodiorite sources in the thorium/scandium vs zirconium/scandium graph, indicating provenance from igneous or metamorphic rocks rather than from the recycling of sedimentary rocks, which would be indicated in case the samples were plotted in the zircon reworking field (Fig. 12B) (Condie, 1993; McLennan et al., 1993).

These samples were also plotted near the andesite compositional field in the thorium/cobalt vs lanthanum/scandium graph (Fig. 12C) (Cullers, 2002) and close to the granodioritic-tonalite field in the thorium/scandium vs europium/europium* diagram (Fig. 12D) (Cullers and Podkovyrov, 2002). In the low-SiO2 DF2 vs DF1 graph, the samples plotted mostly in the collisional field (Fig. 12E) (Verma and Armstrong-Altrin, 2013) and, in the lanthanum/thorium vs hafnium bivariate plot, mostly in the acid island arc source (Fig. 12F) (Floyd and Leveridge, 1987). In the Eu/Eu* vs Gd_{CN}/Yb_{CN} diagram, these samples plotted mostly in the post-Archean field, indicating age similarity between the source areas (Fig. 12G) (McLennan and Taylor, 1991).

6. Conclusions

Authigenic saponite and detrital illite were identified in an 18-meter-thick succession of lutites in the lower Codó Formation, being the first time that an Mg-smectite is reported in the Codó Formation. This clay mineral assemblage, coupled with sedimentological and geochemical information, allowed the identification of a magnesium-sulfate-rich shallow alkaline hypersaline lake with episodes of subaerial exposure. This environment is globally known for having high algal activity, which may explain the high organic matter contents reported in the literature. In addition, hydrothermal processes were interpreted as the magnesium source, which associated with an arid regional climate, caused hypersaline conditions in the lake.

At the top of the alkaline lake succession, a sudden salinity-increasing event was noted and interpreted as the first relevant marine ingression episode in the Codó Formation. This event changed the lake's pH from alkaline to acid, inhibiting the formation of Mg-smectites, and changing its hydrochemical condition, originating a marine-influenced sulfate-rich acid sabkha. This facies succession coincides with a detrital clay mineral assemblage composed of montmorillonite, illite and kaolinite.

At the beginning of the lagoon in the upper Codó Formation, a regional arid to tropical climate humidification process was identified based on clay mineralogical data. It corroborates the hypothesis of the early onset of the equatorial humid belt, which took place due to the proximity between the lake and sea caused by the opening of the equatorial Atlantic Margin during the Gondwana breakup. The lagoon data records the marine-dominated interval of the Codó Formation and are coincident with a detrital clay mineral assemblage composed of kaolinite, montmorillonite and illite. A common post-Archean intermediate source area was also interpreted based on lithogeochemical data from the three environments.

Authigenic saponite was identified in lutites from the alkaline lake in the lower Codó Formation, while stevensite, talc and kerolite compose rocks from the Presalt succession. The geochemical conditions to precipitate these Mg-clay minerals were reached by both systems and involved high pH and high salinity values. However, saponite is an Al-bearing Mg-smectite and its formation process demands a source of Al^{3+}, which is generally associated with inherited detrital Al-bearing clay minerals, such as montmorillonite, kaolinite or illite. It indicates

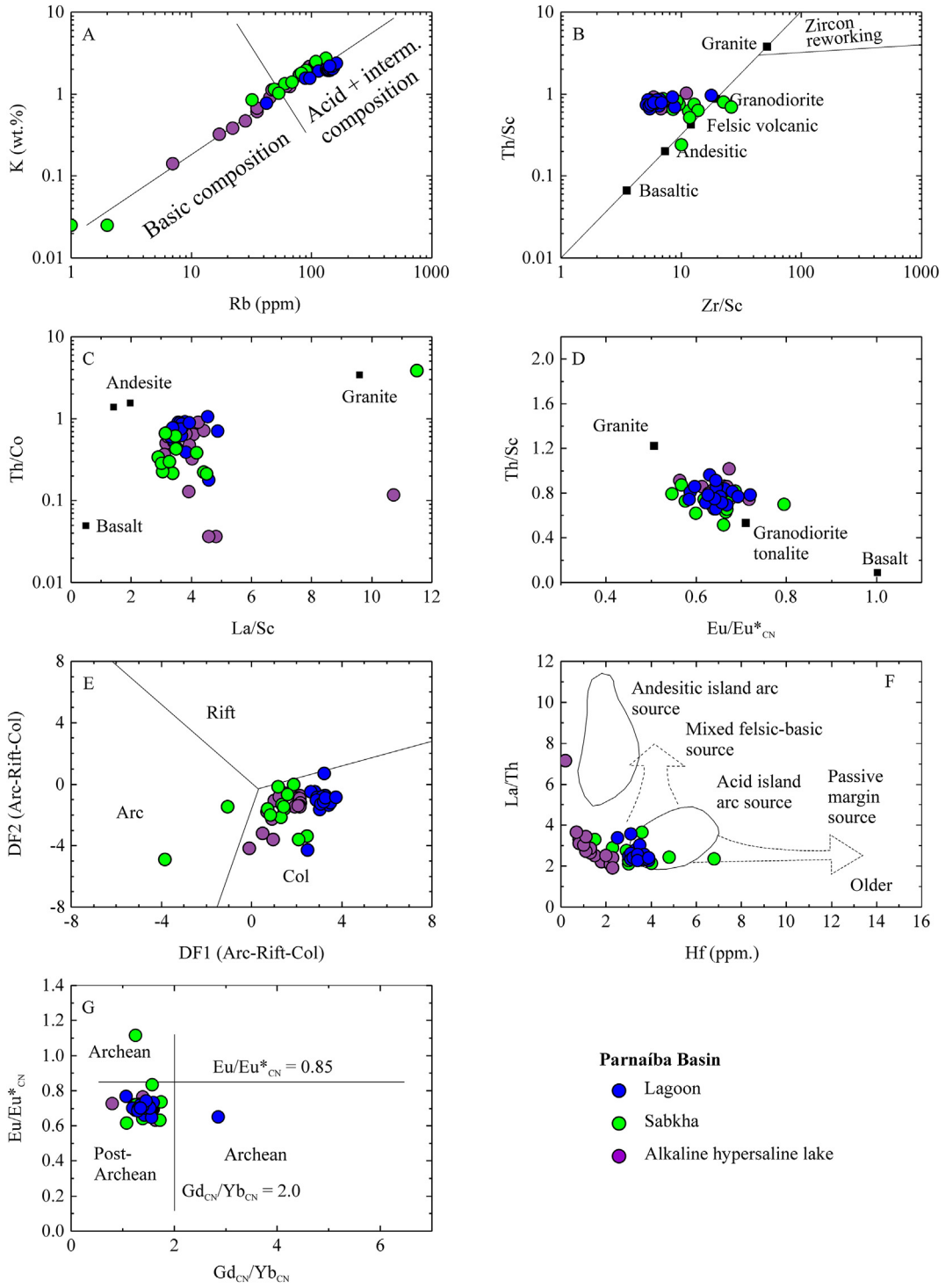

Fig. 12. Lithogeochemical diagrams of composition and tectonic settings of source rocks for the Codó Formation lutites. A) Potassium (wt%) vs rubidium (ppm) graph. B) Thorium/scandium vs zirconium/scandium graph. C) Thorium/cobalt vs lanthanum/scandium graph. D) Thorium/scandium vs europium/europium* graph. E) Low-SiO2 DF2 (Arc-Rift-Col) vs DF1 (Arc-Rift-Col) graph. F) Lanthanum/thorium vs hafnium graph. G) Eu/Eu* vs GdCN/YbCN graph (McLennan and Taylor, 1991).

that the Codó paleolake received a higher sediment supply than the Pre-salt paleolake.

CRediT authorship contribution statement

Victor Matheus Joaquim Salgado-Campos: Conceptualization, Methodology, Validation, Investigation, Writing – original draft, Visualization. **Ismar de Souza Carvalho:** Conceptualization, Investigation, Resources, Writing – review & editing, Supervision, Funding acquisition. **Luiz Carlos Bertolino:** Conceptualization, Resources, Writing – review & editing, Supervision, Funding acquisition. **Leonardo Borghi:** Conceptualization, Investigation, Supervision, Project administration, Funding acquisition. **Aristóteles de Moraes Rios-Netto:** Conceptualization, Investigation, Supervision, Project administration, Funding acquisition. **Bruno Cesar Araújo:** Conceptualization, Investigation, Writing – review & editing. **Danielle Cardoso de Souza:** Conceptualization, Validation,

Investigation, Writing – review & editing. **Laís de Oliveira Ferreira:** Conceptualization, Validation, Investigation, Writing – review & editing. **Fabia Emanuela Rafaloski Bobco:** Conceptualization, Validation, Investigation, Writing – review & editing.

Data availability

Raw data can be found in the supplementary files.

Declaration of competing interest

The authors declare that they have no known competing financial interests or personal relationships that could have appeared to influence the work reported in this paper.

Acknowledgments

The authors thank Shell Brasil Petróleo Ltda for the ongoing R&D project registered as ANP 20.219-2, "Alagoas Project - Stratigraphic correlation, paleo-environmental and paleogeographic evolution and exploratory perspectives of Alagoas Stage" (UFRJ/Shell Brasil/ANP) under the ANP R&D levy as "Compromisso de Investimentos com Pesquisa e Desenvolvimento", the Conselho Nacional de Desenvolvimento Científico e Tecnológico (Brazil) (303596/2016-3), the Fundação Carlos Chagas Filho de Amparo à Pesquisa do Estado do Rio de Janeiro (Brazil) (E-26/200.828/2021; 200.965/2022), the Programa de Pós-graduação em Geologia and the Laboratório de Geologia Sedimentar of the Universidade Federal do Rio de Janeiro (UFRJ) (Brazil) and the Center for Mineral Technology (Brazil). The authors also would like to thank professors Massimo Moretti (editor) and Javier Cuadros (reviewer), and the anonymous reviewers for their comments which helped to improve this manuscript. We thank Guilherme Figueiredo Duarte dos Santos for his contribution during the sampling in the outcrops.

Appendix A. Supplementary data

Supplementary data to this article can be found online at https://doi.org/10.1016/j.sedgeo.2022.106290.

References

Agumanu, A.E., Enu, E.I., 1990. Late Cretaceous clay distribution in the Lower Benue Trough; its palaeoenvironmental and tectonic implication. Journal of African Earth Sciences (and the Middle East) 10 (3), 465–470. https://doi.org/10.1016/0899-5362(90)90099-Z.

Alvarenga, M.V.S., 2010. Fácies orgânica e evolução térmica de uma seção sedimentar da Formação Codó, da Bacia do Parnaíba. Federal University of Rio de Janeiro (End-course thesis. 44 pp.).

Antonioli, L., 2001. Estudo palino-cronoestratigráfico da Formação Codó–Cretáceo inferior do Nordeste brasileiro. Federal University of Rio de Janeiro (Ph.D. thesis. 265 pp.).

Arai, M., 2014. Aptian/Albian (Early Cretaceous) paleogeography of the South Atlantic: a paleontological perspective. Brazilian Journal of Geology 44 (2), 339–350. https://doi.org/10.5327/Z2317-4889201400020012.

Assine, M.L., 2007. Bacia do Araripe. Boletim de Geociencias da Petrobras 15 (2), 371–389.

Bahniuk, A.M., Anjos, S., França, A.B., Matsuda, N., Eiler, J., Mckenzie, J.A., Vasconcelos, C., 2015. Development of microbial carbonates in the Lower Cretaceous Codó Formation (north-east Brazil): implications for interpretation of microbialite facies associations and palaeoenvironmental conditions. Sedimentology 62 (1), 155–181. https://doi.org/10.1111/sed.12144.

Barros, C.L., Silva, S.C., Machado, L.L., Rios-Netto, A.D.M., Sames, B., Alves, T.D., da Silva Júnior, R.P., 2022. Nonmarine ostracods of the Codó Formation (upper Aptian, Lower Cretaceous), Parnaíba Basin, NE Brazil: new biostratigraphic and paleoecological insights. Cretaceous Research 133, 105125. https://doi.org/10.1016/j.cretres.2021.105125.

Barshad, I., 1966. The effect of a variation in precipitation on the nature of clay mineral formation in soils from acid and basic igneous rocks. Proceedings of the International Clay Conference. vol. 2. Israel Programme of Scientific Translation Jerusalem, pp. 167–173.

Bastos, L.P.H., Pereira, E., da Costa Cavalcante, D., Ferreira Alferes, C.L., Jorge de Menezes, C., Rodrigues, R., 2020. Expression of Early Cretaceous Global anoxic events in northeastern Brazilian basins. Cretaceous Research 110, 104390. https://doi.org/10.1016/j.cretres.2020.104390.

Bastos, L.P.H., Jagniecki, E.A., dos Santos, W.H., da Costa Cavalcante, D., de Menezes, C.J., Alferes, C.L.F., da Silva, D.B.N., Bergamaschi, S., Rodrigues, R., Pereira, E., 2022. Organic geochemical evidence for the transition of Aptian–Albian hypersaline environments into marine restricted seas: the South Atlantic oceanic northern gateway and its implications for the pre-salt deposits. Marine and Petroleum Geology 140, 105632. https://doi.org/10.1016/j.marpetgeo.2022.105632.

Bell, C.M., 1989. Saline lake carbonates within an Upper Jurassic–Lower Cretaceous continental red bed sequence in the Atacama region of northern Chile. Sedimentology 36 (4), 651–663. https://doi.org/10.1111/j.1365-3091.1989.tb02091.x.

Bell, C.M., Padian, K., 1995. Pterosaur fossils from the Cretaceous of Chile: evidence for a pterosaur colony on an inland desert plain. Geological Magazine 132 (1), 31–38. https://doi.org/10.1017/S0016756800011407.

Benavides, V., 1962. Saline deposits of South America. In: Mattox, R.B., Holser, W.T., Ode, H., McIntire, W.L., Short, N.M., Taylor, R.E., Van Siclen, D.C. (Eds.), Saline Deposits: A Symposium Based on Papers From the International Conference on Saline Deposits. Geological Society of America, Houston, Texas, pp. 249–290 https://doi.org/10.1130/SPE88-p249.

Birsoy, R., 2002. Formation of sepiolite–palygorskite and related minerals from solution. Clays and Clay Minerals 50 (6), 736–745. https://doi.org/10.1346/000986002762090263.

Biscaye, P.E., 1965. Mineralogy and sedimentation of recent deep-sea clay in the Atlantic Ocean and adjacent seas and oceans. Geological Society of America Bulletin 76 (7), 803–832. https://doi.org/10.1130/0016-7606(1965)76[803:MASORD]2.0.CO;2.

Boucot, A.J., Xu, C., Scotese, C.R., Morley, R.J., 2013. Phanerozoic paleoclimate: an atlas of lithologic indicators of climate. SEPM Concepts in Sedimentology and Paleontologyvol. 11. https://doi.org/10.2110/sepmcsp.11.

Brigatti, M.F., Guidotti, C.V., Malferrari, D., Sassi, F.P., 2008. Single-crystal X-ray studies of trioctahedral micas coexisting with dioctahedral micas in 581 metamorphic sequences from western Maine. American Mineralogist 93 (2–3), 396–408. https://doi.org/10.2138/am.2008.2523.

Brindley, G.W., Brown, G., 1980. Quantitative X-ray mineral analysis of clays. In: Brindley, G.W., Brown, G. (Eds.), Crystal Structures of Clay Minerals and their X-ray Identificationvol. 5, pp. 411–438. https://doi.org/10.1180/mono-5.7.

Bristow, T.F., Derkowski, A., Blake, D.F., Berlanga, G., De Deckker, P., 2021. A comparative study of clay mineral authigenesis in terrestrial and martian lakes; an Australian example. American Journal of Science 321 (7), 1080–1110. https://doi.org/10.2475/07.2021.03.

Brownfield, M.E., Weaver, J.N., 1992. Paleogeography and stratigraphy of Cretaceous coal deposits of North Africa. In: McCabe, P.J., Parrish, J.T. (Eds.), Controls on the Distribution and Quality of Cretaceous Coals. The Geological Society of America Special Paper 267, pp. 369–384 https://doi.org/10.1130/SPE267-p369.

Bueno, G.V., Zacharias, A.A., Oreiro, S.G., Cupertino, J.A., Falkenhein, F.U.H., Martins Neto, M.A., 2007. Bacia de Pelotas. Boletim de Geociencias da Petrobras 15 (2), 551–559.

Caixeta, J.M., da Silva Milhomen, P., Witzke, R.E., Dupuy, I.S.S., Gontijo, G.A., 2007. Bacia de Camamu. Boletim de Geociencias da Petrobras v, 15.

Calvo, J.P., Pozo, M., 2015. Geology of magnesian clays in sedimentary and non-sedimentary environments. In: Pozo, M., Galán, E. (Eds.), Magnesian Clays: Characterization, Origin and Applications. AIPEA Educational Series, Pub. No. 2. Digilabs, Bari, Italy, Madri Basin (Spain), pp. 123–174.

Campbell, D.F., 1949. Revised Report on the Reconnaissance Geology of the Maranhão Basin. Rio de Janeiro, Conselho Nacional do Petróleo. Relatório Interno (117 pp.).

Campbell, F.A., Lerbekmo, J.F., 1963. Mineralogic and chemical variations between Upper Cretaceous continental Belly River shales and marine Wapiabi shales in western Alberta, Canada. Sedimentology 2 (3), 215–226. https://doi.org/10.1111/j.1365-3091.1963.tb01215.x.

Campbell, F.A., Williams, G.D., 1965. Chemical composition of shales of Mannville group (lower Cretaceous) of central Alberta, Canada. AAPG Bulletin 49 (1), 81–87. https://doi.org/10.1306/A66334EA-16C0-11D7-8645000102C1865D.

Campos Neto, O., Lima, W.S., Cruz, F.G., 2007. Bacia de Sergipe-Alagoas. Boletim de Geociencias da Petrobras 15 (2), 405–415.

Carbonell, V.V.R., Collo, G., Wunderlin, C.A., Alasino, P.H., Ciccioli, P.L., Rocher, S., Maza, S., 2022. Clay mineral assemblages as indicators of paleoenvironmental and diagenetic dynamics in the Neogene Fiambalá Basin, NW Argentina. Journal of South American Earth Sciences 118, 103949. https://doi.org/10.1016/j.jsames.2022.103949.

Carrado, K.A., Decarreau, A., Petit, S., Bergaya, F., Lagaly, G., 2006. Synthetic clay minerals and purification of natural clays. In: Begaya, F., Theng, B.K.G., Lagaly, G. (Eds.), Handbook of Clay Science. Developments in Clay Sciencevol. 1, pp. 115–140.

Carramal, N.G., Oliveira, D.M., Cacela, A.S., Cuglieri, M.A., Rocha, N.P., Viana, S.M., Toledo, S. L.V., de Pedrinha, S., Ros, L.F., 2022. Paleoenvironmental insights from the deposition and diagenesis of Aptian pre-salt magnesium silicates from the Lula Field, Santos Basin, Brazil. Journal of Sedimentary Research 92 (1), 12–31. https://doi.org/10.2110/jsr.2020.139.

Carvalho, I.S., de Gasparini, Z.B., Salgado, L., de Vasconcellos, F.M., da Silva Marinho, T., 2010. Climate's role in the distribution of the Cretaceous terrestrial Crocodyliformes throughout Gondwana. Palaeogeography, Palaeoclimatology, Palaeoecology 297 (2), 252–262. https://doi.org/10.1016/j.palaeo.2010.08.003.

Carvalho, M.A., Bengtson, P., Lana, C.C., de Paula Sá, N., Santiago, G., da Silva Giannerini, M.C., 2019. Late Aptian (Early Cretaceous) dry–wet cycles and their effects on vegetation in the South Atlantic: palynological evidence. Cretaceous Research 100, 172–183. https://doi.org/10.1016/j.cretres.2019.03.021.

Cerqueira, J.R., Marques, L.P., 1985. Avaliação geoquímica da bacia de São Luís. Boletim Tecnico da Petrobras 28 (3), 151–158.

Chamley, H., 1989. Clay Mineralogy. Springer, Paris (626 pp.).

Chase, J.E., Arizaleta, M.L., Tutolo, B.M., 2021. A series of data-driven hypotheses for inferring biogeochemical conditions in alkaline lakes and their deposits based on the behavior of Mg and SiO2. Minerals 11 (2), 106. https://doi.org/10.3390/min11020106.

Cheary, R.W., Coelho, A., 1992. A fundamental parameters approach to X-ray 590 line-profile fitting. Journal of Applied Crystallography 25 (2), 109–112. https://doi.org/10.1107/S0021889891010804.
Christidis, G.E., Koutsopoulou, E., 2013. A simple approach to the identification of trioctahedral smectites by X-ray diffraction. Clay Minerals 48 (5), 687–696. https://doi.org/10.1180/claymin.2013.048.5.22.
Chumakov, N.M., Zharkov, M.A., Herman, A.B., Doludenko, M.P., Kalandadze, N.N., Lebedev, E.A., Ponomarenko, A.G., Rautian, A.S., 1995. Climate belts of the Mid Cretaceous time. Stratigraphy and Geological Correlation 3 (3), 241–260.. https://oceanrep.geomar.de/id/eprint/37939.
Cohen, A.S., 2003. Paleolimnology: The History and Evolution of Lake Systems. Oxford University Press (525 pp.).
Coimbra, R., Rocha, F., Immenhauser, A., Olóriz, F., Terroso, D., Horikx, M., 2021. Carbonate-hosted clay minerals: a critical re-evaluation of extraction methods and their possible bias on palaeoenvironmental information. Earth-Science Reviews 214, 103502. https://doi.org/10.1016/j.earscirev.2021.103502.
Condie, K.C., 1993. Chemical composition and evolution of the upper continental crust: contrasting results from surface samples and shales. Chemical Geology 104 (1–4), 1–37. https://doi.org/10.1016/0009-2541(93)90140-E.
Congleton, J.D., 1990. Vertebrate Paleontology of the Koum Basin, Northern Cameroon, and Archosauian Paleobiogeography in the Early Cretaceous. Southern Methodist University (Unpublished M.Sc. thesis, 258 pp.).
Córdoba, V.C., Jardim de Sá, E.F., Sousa, D.C., Antunes, A.F., 2007. Bacia de Pernambuco-Paraíba. Boletim de Geociencias da Petrobras 15 (2), 391–403.
Coura, A.P.P., 2011. Caracterização faciológica e paleoambiental de estromatólitos da Formação Codó (Aptiano, Bacia do Parnaíba). Federal University of Rio de Janeiro (M.Sc. thesis. 114 pp.).
Coward, M.P., Purdy, E.G., Ries, A.C., Smith, D.G., 1999. The distribution of petroleum reserves in basins of the South Atlantic margins. In: Cameron, N.R., Bate, R.H., Clure, V.S. (Eds.), The Oil and Gas Habitats of the South Atlantic. Geological Society (London) Special Publication 153, pp. 101–131.
Craigie, N.W., 2018. Principles of Elemental Chemostratigraphy. Springer, Switzerland (196 pp.).
Cronin, T.M., 1999. Principles of Paleoclimatology. Columbia University Press, New York (575 pp.).
Cullers, R.L., 2002. Implications of elemental concentrations for provenance, redox conditions, and metamorphic studies of shales and limestones near Pueblo, CO, USA. Chemical Geology 191 (4), 305–327. https://doi.org/10.1016/S0009-2541(02)00133-X.
Cullers, R.L., Podkovyrov, V.N., 2002. The source and origin of terrigenous sedimentary rocks in the Mesoproterozoic Ui group, southeastern Russia. Precambrian Research 117 (3–4), 157–183. https://doi.org/10.1016/S0301-9268(02)00079-7.
Darragi, F., Tardy, Y., 1987. Authigenic trioctahedral smectites controlling pH, alkalinity, silica and magnesium concentrations in alkaline lakes. Chemical Geology 63 (1–2), 59–72. https://doi.org/10.1016/0009-2541(87)90074-X.
De Ruiter, P.A.C., 1979. The Gabon and Congo basins salt deposits. Economic Geology 74 (2), 419–431. https://doi.org/10.2113/gsecongeo.74.2.419.
Deocampo, D.M., 2004. Authigenic clays in East Africa: regional trends and paleolimnology at the Plio–Pleistocene boundary, Olduvai Gorge, Tanzania. Journal of Paleolimnology 31 (1), 1–9. https://doi.org/10.1023/B:JOPL.0000013353.86120.9b.
Deocampo, D.M., 2005. Evaporative evolution of surface waters and the role of aqueous CO2 in magnesium silicate precipitation: Lake Eyasi and Ngorongoro Crater, northern Tanzania. South African Journal of Geology 108 (4), 493–504. https://doi.org/10.2113/108.4.493.
Deocampo, D.M., 2015. Authigenic clay minerals in lacustrine mudstones. Geological Society of America Special Papers 515, SPE515-03. https://doi.org/10.1130/2015.2515(03).
Dias, J.L., Sad, A.R.E., Fontana, R.L., Feijó, F.J., 1994. Bacia de Pelotas. Boletim de Geociencias da Petrobras 8 (1), 235–245.
Dias, I.A., Cury, L.F., Titon, B.G., Athayde, G.B., Fedalto, G., da Rocha Santos, L., Soares, A.P., Athayde, C.V.M., Bahniuk Rumbeslperger, A.M., 2020. The occurrence of authigenic clay minerals in alkaline-saline lakes, Pantanal Wetland (Nhecolândia Region, Brazil). Minerals 10 (8), 718. https://doi.org/10.3390/min10080718.
Dietz, R.S., Holden, J.C., 1970. Reconstruction of Pangaea: breakup and dispersion of continents, Permian to present. Journal of Geophysical Research 75 (26), 4939–4956. https://doi.org/10.1029/JB075i026p04939.
Dingle, R.V., Siesser, W.G., Newton, A.R., 1983. Mesozoic and Tertiary Geology of Southern Africa. Routledge & CRC Press Balkema (384 pp.).
Dyni, J.R., 1976. Trioctahedral Smectite in the Green River Formation, Duchesne County, Utah (No. 967). USGS https://doi.org/10.3133/pp967.
Emsbo, P., Seal, R.R., Breit, G.N., Diehl, S.F., Shah, A.K., 2016. Sedimentary Exhalative (Sedex) Zinc–Lead–Silver Deposit Model (No. 2010-5070-N). USGS https://doi.org/10.3133/sir20105070N.
Enu, E.I., 1980. Sukuliye (Sekule) Formation; facies equivalent of the Numanha Formation in the Upper Benue Trough. Nigeria. Journal of Mining and Geology 17, 91–95.
Feijó, F.J., 1994. Sergipe and Alagoas Basins; Bacias de Sergipe e Alagoas. Boletim de Geociencias da Petrobras 8.
Fernandes, G., Piazza, H.D., 1978. O potencial oleogenítico da Formação Codó. Boletim tecnico da Petrobras 21 (1), 3–16.
Ferreira, N.N., Ferreira, E.P., Ramos, R.R., Carvalho, I.D.S., 2020. Terrestrial and marine palynomorphs from deposits of the pull-apart rift of West Gondwana (Parnaíba Basin, northern Brazil): biostratigraphy and relation to tectonic events. Journal of South American Earth Sciences 101, 102612. https://doi.org/10.1016/j.jsames.2020.102612.
Floyd, P.A., Leveridge, B.E., 1987. Tectonic environment of the Devonian Gramscatho basin, south Cornwall: framework mode and geochemical evidence from turbiditic sandstones. Journal of the Geological Society 144 (4), 531–542. https://doi.org/10.1144/gsjgs.144.4.0531.
França, L.R., Del Rey, A.C., Tagliari, C.V., Brandão, J.R., Fontanelli, P.R., 2007. Bacia de Mucuri. Boletim de Geociencias da Petrobras 15 (2), 493–499.
Furquim, S.A.C., 2007. Formação de carbonatos e argilo-minerais em solos sódicos do Pantanal Sul-Mato-Grossense. University of São Paulo (Ph.D. thesis. 222 pp.).
Furquim, S.A.C., Graham, R.C., Barbiero, L., de Queiroz Neto, J.P., Vallès, V., 2008. Mineralogy and genesis of smectites in an alkaline-saline environment of Pantanal wetland, Brazil. Clays and Clay Minerals 56 (5), 579–595. https://doi.org/10.1346/CCMN.2008.0560511.
Galán, E., Pozo, M., 2011. Palygorskite and sepiolite deposits in continental environments. Description, genetic patterns and sedimentary settings. In: Galàn, E., Singer, A. (Eds.), Developments in Clay Science. vol. 3. Elsevier, pp. 125–173.
Geiger, M., 2000. The Geology of the Southern Warmbad Basin Margin-Tephrostratigraphy, Age, Fossil Record and Sedimentary Environment of Carboniferous-Permian Glacigenic Deposits of the Dwyka Group, Zwartbas, Southern Namibia. Universität Würzburg (Ph.D. thesis).
Germann, K., Fischer, K., Schwarz, T., 1990. Accumulation of lateritic weathering products (kaolins, bauxitic laterites, ironstones) in sedimentary basins in northern Sudan. Berliner geowissenschaftliche Abhandlungen / A 120 (1), 109–148.
Góes, A.M., Feijó, F.J., 1994. Bacia do Parnaíba. Boletim de Geociencias da Petrobras 8 (1), 57–67.
Gonçalves, D.F., Rossetti, D.F., Truckenbrodt, W., Mendes, A.C., 2006. Argilominerais da Formação Codó (Aptiano Superior), Bacia de Grajaú, Nordeste do Brasil. Latin American Journal of Sedimentology and Basin Analysis 13 (1), 59–75.
Gontijo, G.A., Milhomem, P.S., Caixeta, J.M., Dupuy, I.S.S., Menezes, P.E.L., 2007. Bacia de Almada. Boletim de Geociencias da Petrobras 15 (2), 463–473.
Goodyear, J., Duffin, W.J., 1961. An X-ray examination of an exceptionally well crystallized kaolinite. Mineralogical Magazine and Journal of the Mineralogical Society 32 (254), 902–907. https://doi.org/10.1180/minmag.1961.032.254.05.
Graddi, J.C.S.V., Campos Neto, O.P.D.A., Caixeta, J.M., 2007. Bacia de Jacuípe. Boletim de Geociencias da Petrobras 15 (2), 417–421.
Greigert, J., 1966. Description des formations crétacées et tertiaires du Bassin des Tullemmeden (Afrique occidentale). République du Niger, Direction de Mines et de la Géologie, Publication, (2).
Grimaldi, D.A., Maisey, J.G., McCafferty, W.P., Carle, F.L., Wighton, D.C., Popham, E.J., Krishna, E.J., Hamilton, K.G.A., Darling, D.C., Sharkey, M.J., Oswald, J.D., 1990. Insects from the Santana Formation, Lower Cretaceous, of Brazil. Bulletin of the American Museum of Natural History 195.. http://hdl.handle.net/2246/943.
Guerra-Sommer, M., Degani-Schmidt, I., Mendonça, J.O., Mendonça Filho, J.G., Lopes, F.D.S., Salgado-Campos, V.M.J., Araújo, B., Carvalho, I.S., 2021. Multidisciplinary approach as a key for paleoenvironmental interpretation in a Weichselia-dominant interval from the late Aptian Codó Formation (Parnaíba Basin, Brazil). Journal of South American Earth Sciences 111, 103490. https://doi.org/10.1016/j.jsames.2021.103490.
Guggenheim, S., Adams, J.M., Bain, D.C., Bergaya, F., Brigatti, M.F., Drits, V.A., Formoso, L.L., Galán, E., Kogure, T., Stanjek, H., 2006. Summary of recommendations of nomenclature committees relevant to clay mineralogy: report of the Association Internationale pour l'Etude des Argiles (AIPEA) Nomenclature Committee for 2006. Clays and Clay Minerals 54 (6), 761–772. https://doi.org/10.1346/CCMN.2006.0540610.
Harris, N.B., Mello, M.R., Katz, B.J., 2000. Toca Carbonate, Congo Basin: response to an evolving rift lake. Memoirs-American Association of Petroleum Geologists, pp. 341–360 https://doi.org/10.1306/M73705C24.
Hartley, A.J., Flint, S., Turner, P., Jolley, E.J., 1992. Tectonic controls on the development of a semiarid alluvial basin as reflected in the stratigraphy of the Purilactis Group (upper cretaceous-eocene), northern Chile. Journal of South American Earth Sciences 5 (3–4), 275–296. https://doi.org/10.1016/0895-9811(92)90026-U.
Hay, W.W., Floegel, S., 2012. New thoughts about the Cretaceous climate and oceans. Earth-Science Reviews 115 (4), 262–272. https://doi.org/10.1016/j.earscirev.2012.09.008.
Heimhofer, U., Ariztegui, D., Lenniger, M., Hesselbo, S.P., Martill, D.M., Rios-Netto, A.M., 2010. Deciphering the depositional environment of the laminated Crato fossil beds (Early Cretaceous, Araripe Basin, North-eastern Brazil). Sedimentology 57 (2), 677–694. https://doi.org/10.1111/j.1365-3091.2009.01114.x.
Hover, V.C., Ashley, G.M., 2003. Geochemical signatures of paleodepositional and diagenetic environments: a STEM/AEM study of authigenic clay minerals from an arid rift basin, Olduvai Gorge, Tanzania. Clays and Clay Minerals 51 (3), 231–251. https://doi.org/10.1346/CCMN.2003.0510301.
Hussain, S.H., Al-Juboury, A.I., Al-Haj, M.A., Armstrong-Altrin, J.S., Al-Lhaebi, S.F., 2021. Mineralogy and geochemistry of the Late Triassic Baluti Formation, Northern Iraq. Journal of African Earth Sciences 181, 104243. https://doi.org/10.1016/j.jafrearsci.2021.104243.
International Centre for Diffraction Data PDF4+ (ICDD), 2012. Newton Square, USA.
Javor, B.J., 2012. Hypersaline Environments: Microbiology and Biogeochemistry. Springer, New York (336 pp.).
Jones, B., 1948. Sedimentary rocks of Sokoto Province. Bulletin of the Geological Survey of Nigeria 18 (79 pp.).
Jones, B.F., Weir, A.H., 1983. Clay minerals of Lake Abert, an alkaline, saline lake. Clays and Clay Minerals 31 (3), 161–172. https://doi.org/10.1346/CCMN.1983.0310301.
Joulia, F., 1959. Les series primaires au N et NW de l'Air (Sahara central); discordances observees. Bulletin de la Societe Geologique de France 7 (2), 192–196. https://doi.org/10.2113/gssgfbull.S7-I.2.192.
Joulia, F., Bonifas, M., Weil, R., Camez, T., Millot, G., 1958. Analcimolites sédimentaires dans le Continental Intercalaire du Sahara central (Bassin du Niger, AO F). Sciences Geologiques, Bulletins et Memoires 11 (2), 67–70. https://doi.org/10.3406/sgeol.1958.1190.

Katz, B.J., Mello, M.R., 2000. Petroleum systems of South Atlantic Marginal basins-an overview. Memoirs-American Association of Petroleum Geologists, pp. 1–14 https://doi.org/10.1306/M73705C1.
Keller, W.D., 1978. Classification of kaolins exemplified by their textures in scan electron micrographs. Clays and Clay Minerals 26 (1), 1–20. https://doi.org/10.1346/CCMN.1978.0260101.
Kern, A., Eysel, W., 1993. Mineralogisch-Petrograph. Institute, University of Hidelberg, Germany (ICDD Grant-in-Aid).
Leite, J.F., Aboarrage, A.M., Daemon, R.F., 1975. Projeto carvão da Bacia do Parnaíba. Relatório Final das Etapas II e III, DNPM/CPRM, Recife.
Lima, M.R., 1983. Palinologia da Formação Codó na região de Codó, Maranhão. Boletim do Instituto de Geociencias da USP 13, 116–128. https://doi.org/10.11606/issn.2316-8978.v13i0p116-128.
Lima, B.E.M., De Ros, L.F., 2019. Deposition, diagenetic and hydrothermal processes in the Aptian Pre-Salt lacustrine carbonate reservoirs of the northern Campos Basin, offshore Brazil. Sedimentary Geology 383, 55–81. https://doi.org/10.1016/j.sedgeo.2019.01.006.
Lima, H.P., Aranha, L.G.F., Feijó, F.J., 1994. Bacias de Bragança-Viseu, São Luíz e Graben de Ilha Nova. Boletim de Geociencias da Petrobras 8 (1), 111–116.
Lindoso, R.M., Carvalho, I.S., Mendes, I.D., 2013. An Isopod from the Codó Formation (Aptian of the Parnaíba Basin), Northeastern Brazil. Brazilian Journal of Geology 43 (1), 16–21. https://doi.org/10.5327/Z2317-48892013000100003.
Lindoso, R.M., Maisey, J.G., Carvalho, I.S., 2016. Ichthyofauna from the Codó Formation, Lower Cretaceous (Aptian, Parnaíba Basin), Northeastern Brazil and their paleobiogeographical and paleoecological significance. Palaeogeography, Palaeoclimatology, Palaeoecology 447 (2016), 53–64. https://doi.org/10.1016/j.palaeo.2016.01.045.
Lisboa, M.A.R., 1914. The Permian geology of Northern Brazil. American Journal of Science 4 (37), 425–443.
Maizatto, J.R., Queiroz Neto, J.V., Ferreira, E.P., Bahniuk, A.M., 2011. Palinomorfos e ostracodes não marinhos de afloramentos da Formação Codó, Bacia do Parnaíba. In: Carvalho, I.S., Garcia, M.J., Lana, C.C., Stronhschoen Jr., O. (Eds.), Paleontologia: Cenários de Vida – Paleoclimas. vol. 5. Editora Interciência, 378, p. 367.
Martill, D.M., 1993. Fossils of the Santana and Crato Formations, Brazil. Palaeontological Association (160 pp.).
Matos, R.M.D., Krueger, A., Norton, I., Casey, K., 2021a. The fundamental role of the Borborema and Benin–Nigeria provinces of NE Brazil and NW Africa during the development of the South Atlantic Cretaceous Rift system. Marine and Petroleum Geology 127, 104872. https://doi.org/10.1016/j.marpetgeo.2020.104872.
Matos, R.M.D., Medeiros, W.E., de Sá, E.F.J., de Almeida, C.B., Norton, I., Córdoba, V.C., 2021b. A solution to the Albian fit challenge between the South American and African plates based on key magmatic and sedimentary events late in the rifting phase in the Pernambuco and Paraíba basins. Marine and Petroleum Geology 128, 105038. https://doi.org/10.1016/j.marpetgeo.2021.105038.
McLachlan, I.R., McMillan, I.K., 1976. Review and stratigraphic significance of southern Cape Mesozoic palaeontology. South African Journal of Geology 79 (2), 197–212.. https://hdl.handle.net/10520/AJA10120750_2859.
McLaughlin Jr., D.H., 1972. Evaporite deposits of Bogotá area, cordillera oriental, Colombia. AAPG Bulletin 56 (11), 2240–2259. https://doi.org/10.1306/819A41FE-16C5-11D7-8645000102C1865D.
McLennan, S.M., 2001. Relationships between the trace element composition of sedimentary rocks and upper continental crust. Geochemistry, Geophysics, Geosystems 2 (4). https://doi.org/10.1029/2000GC000109.
McLennan, S.M., Taylor, S.R., 1991. Sedimentary rocks and crustal evolution: tectonic setting and secular trends. The Journal of Geology 99 (1), 1–21.. https://www.jstor.org/stable/30068762.
McLennan, S.M., Hemming, S., McDaniel, D.K., Hanson, G.N., 1993. Geochemical approaches to sedimentation, provenance, and tectonics. Special Papers-Geological Society of America. In: Johnsson, M.J., Basu, A. (Eds.), Processes Controlling the Composition of Clastic Sediments, pp. 21–40.
McMillan, I.K., Brink, G.I., Broad, D.S., Maier, J.J., 1997. Late Mesozoic sedimentary basins off the south coast of South Africa. In: Selley, R.C. (Ed.), Sedimentary Basins of the World. vol. 3. Elsevier, pp. 319–376. https://doi.org/10.1016/S1874-5997(97)80016-0.
Mendes, M.S., 2007. Análise estratigráfica do intervalo formacional Grajaú-Codó (Aptiano) da Bacia do Parnaíba, NE do Brasil. Federal University of Rio de Janeiro (M.Sc. thesis. 164 pp.).
Mesner, J.C., Wooldridge, L.P., 1962. The Maranhão Basin Study Revision. Petrobrás, Belém, DEPEX/SEDOC 103-00645, 2 v.
Mesner, J.C., Wooldridge, L.P., 1964. Maranhão Paleozoic basin and Cretaceous coastal basins, north Brazil. AAPG Bulletin 48 (9), 1475–1512.
Meunier, A., 2005. Clays. Springer, Poitiers (476 pp.).
Moody, R.T.J., 1997. The Iullemmeden Basin. In: Selley, R.C. (Ed.), African Basins. Sedimentary Basins of the World. vol. 3. Elsevier, Amsterdam, pp. 89–103.
Moody, R.T.J., Sutcliffe, P.J.C., 1991. The Cretaceous deposits of the Iullemmeden basin of Niger, central West Africa. Cretaceous Research 12 (2), 137–157. https://doi.org/10.1016/S0195-6671(05)80021-7.
Moore, D.M., Reynolds, R.C., 1997. X-ray Diffraction and the Identification and Analysis of Clay Minerals. Oxford University Press, Oxford (392 pp.).
Moreira, J.L.P., Madeira, C.V., Gil, J.A., Machado, M.A.P., 2007. Bacia de Santos. Boletim de Geociencias da Petrobras 15 (2), 531–549.
Nesbitt, H.W., Young, G.M., 1984. Prediction of some weathering trends of plutonic and volcanic rocks based on thermodynamic and kinetic considerations. Geochimica et Cosmochimica Acta 48 (7), 1523–1534. https://doi.org/10.1016/0016-7037(84)90408-3.
Netto, A.S.T., Wanderley Filho, J.R., Feijó, F.J., 1994. Bacias de Jacuípe, Camamu e Almada. Boletim de Geociencias da Petrobras 8 (1), 173–184.
Netto, P.R.A., Pozo, M., da Silva, M.D., Mexias, A.S., Gomes, M.E.B., Borghi, L., Rios-Netto, A.M., 2022. Authigenic Mg-clay assemblages in the Barra Velha Formation (Upper Cretaceous) from Santos Basin (Brazil): the role of syngenetic and diagenetic process. Applied Clay Science 216, 106339.
Neves, I.A.N., 2007. Aplicação da palinofacies na caracterização paleoambiental da Formação Codó, Cretáceo da Bacia do Parnaíba. Federal University of Rio de Janeiro (End-course thesis. 41 pp.).
Oliveira, N.S., Schiavo, J.A., de Souza, A.C., Laranjeira, L.T., de Moraes, E.M.V., Pereira, M.G., 2021. Mineralogy and genesis in an alkaline soil system in the southern Pantanal wetland, Brazil. Journal of South American Earth Sciences 111, 103456. https://doi.org/10.1016/j.jsames.2021.103456.
Paz, J.D.S., Rossetti, D.F., 2001. Reconstrução paleoambiental da Formação Codó (Aptiano), borda leste da Bacia do Grajaú, MA. In: Rossetti, D.F., Góes, A.M., Truckenbrodt, W. (Eds.), O Cretáceo na Bacia de São Luís-Grajaú. Coleção Friedrich Katzer Ed. Museu Paraense Emílio Goeldi, Belém, pp. 77–100.
Paz, J.D.S., Rossetti, D.F., Macambira, M.J.B., 2005. An Upper Aptian saline pan/lake system from the Brazilian equatorial margin: integration of facies and isotopes. Sedimentology 52, 1303–1321. https://doi.org/10.1111/j.1365-3091.2005.00744.x.
Pedrão, E., Barrilari, I.M.R., Lima, H.P., 1993. Estudos palinológicos dos sedimentos cretácicos da Bacia do Parnaíba. Relatório Interno, Petrobras/Cenpes/Divex/Sebipe.
Pereira, M.J., Feijó, F.J., 1994. Bacia de Santos. Boletim de Geociencias da Petrobras 8.
Petri, S., 1983. Brazilian Cretaceous paleoclimates: evidence from clay minerals, sedimentary structures and palynomorphs. Revista Brasileira de Geociencias 13 (4), 215–222.
Pirajno, F., 2012. Hydrothermal Mineral Deposits: Principles and Fundamental Concepts for the Exploration Geologist. Springer (1282 pp.).
Ponte, F.C., Appi, C.J., 1990. Proposta de revisão da coluna litoestratigráfica da Bacia do Araripe. Congresso Brasileiro de Geologia 36, Natal, pp. 211–226.
Pourmand, A., Dauphas, N., Ireland, T.J., 2012. A novel extraction chromatography and MC-ICP-MS technique for rapid analysis of REE, Sc and Y: revising CI-chondrite and Post-Archean Australian Shale (PAAS) abundances. Chemical Geology 291, 38–54. https://doi.org/10.1016/j.chemgeo.2011.08.011.
Pozo, M., Calvo, J.P., 2018. An overview of authigenic magnesian clays. Minerals 8 (11), 520. https://doi.org/10.3390/min8110520.
Pozo, M., Galán, E., 2015. Magnesian clays – characterization, origin and applications (pub. no. 2). AIPEA Educational Series (Italy, 397 pp.).
Ramstein, G., Landais, A., Bouttes, N., Sepulchre, P., Govin, A., 2020. Paleoclimatology. Springer (485 pp.).
Rangel, H.D., Martins, F.A.L., Esteves, F.R., Feijó, F.J., 1994. Bacia de Campos. Boletim de Geociencias da Petrobras 8 (1), 203–217.
Rangel, H.D., Oliveira, J.L.F., Caixeta, J.M., 2007. Bacia de Jequitinhonha. Boletim de Geociencias da Petrobras 15 (2), 475–483.
Regali, M.S.P., Santos, P.S., 1999. Palinoestratigrafia e geocronologia dos sedimentos albo-aptianos das Bacias de Sergipe e Alagoas–Brasil. Simposio Sobre o Cretaceo do Brasil 5, 411–419.
Rehim, H.A.A.A., Mizusaki, A.M.P., Carvalho, M.D., Monteiro, M., 1986. Talco e estevensita na Formação Lagoa Feia da bacia de Campos-possíveis implicações no ambiente deposicional. Anais XXXIV Congresso Brasileiro de Geologia pp. 416–422.
Rezende, O.M., Pamplona, H.R.P., 1970. Estudo do desenvolvimento do arco Ferrer-Urbano Santos. Boletim Tecnico da Petrobras 13, 5–14.
Riccardi, A.C., 1988. The Cretaceous system of southern south America 168. Geological Society of America https://doi.org/10.1130/MEM168-p1.
Richetti, P.C., Schmitt, R.S., Reeves, C., 2018. Dividing the South American continent to fit a Gondwana reconstruction: a model based on continental geology. Tectonophysics 747, 79–98. https://doi.org/10.1016/j.tecto.2018.09.011.
Robb, L., 2020. Introduction to Ore-forming Processes. John Wiley & Sons (496 pp.).
Rodovalho, N., Gontijo, R.C., Santos, C.F., Milhomem, P.S., 2007. Bacia de Cumuruxatiba. Boletim de Geociencias da Petrobras 15 (2), 485–491.
Rodrigues, R., 1995. A geoquímica orgânica da Bacia do Parnaíba. Federal University of the Rio Grande do Sul (Ph.D. thesis. 225 pp.).
Rona, P.A., 1982. Evaporites at passive margins. Dynamics of Passive Margins 6, 116–132. https://doi.org/10.1029/GD006p0116.
Rossetti, D.F., Góes, A.M., 2000. Deciphering the sedimentological imprint of paleoseismic events: an example from the Aptian Codó Formation, northern Brazil. Sedimentary Geology 135 (1–4), 137–156. https://doi.org/10.1016/S0037-0738(00)00068-3.
Rossetti, D.F., Truckenbrodt, W., Santos Júnior, A.E., 2001. Clima do Cretáceo no Meio-norte brasileiro. In: Rossetti, D.F., Góes, A.M., Truckenbrodt, W. (Eds.), O Cretáceo na Bacia de São Luís-Grajaú. Coleção Friedrich Katzer Ed. Museu Paraense Emílio Goeldi, Belém, pp. 67–76.
Rossetti, D.F., Paz, J.D., Góes, A.M., 2004. Facies analysis of the Codó formation (late Aptian) in the Grajaú area, southern São Luís-Grajaú Basin. Anais da Academia Brasileira de Ciências 76 (4), 791–806. https://doi.org/10.1590/S0001-37652004000400012.
Salgado, L., Coria, R.A., Heredia, S.E., 1997. New materials of Gasparinisaura cincosaltensis (Ornithischia, Ornithopoda) from the Upper Cretaceous of Argentina. Journal of Paleontology 71 (5), 933–940.
Salgado-Campos, V.M.J., Carvalho, I.S., Bertolino, L.C., Duarte, T.A., Araújo, B.C., Borghi, L., 2021. Clay mineralogy and lithogeochemistry of lutites from the Lower Cretaceous Crato Member, Araripe Basin, NE Brazil: implications for paleoenvironmental, paleoclimatic and provenance reconstructions. Journal of South American Earth Sciences 110, 103329. https://doi.org/10.1016/j.jsames.2021.103329.
Saller, A., Rushton, S., Buambua, L., Inman, K., McNeil, R., Dickson, J.T., 2016. Presalt stratigraphy and depositional systems in the Kwanza Basin, offshore Angola. AAPG Bulletin 100 (7), 1135–1164. https://doi.org/10.1306/02111615216.
Santos, C.F., Gontijo, R.C., Araújo, M.B., Feijó, F.J., 1994. Bacias de Cumuruxatiba e Jequitinhonha. Boletim de Geociencias da Petrobras 8 (1), 185–190.

Santos, H.N., Neumann, R., Ávilla, C.A., 2017. Mineral quantification with simultaneous refinement of Ca–Mg carbonates non-stoichiometry by X-ray diffraction, Rietveld method. Minerals 7 (9), 164. https://doi.org/10.3390/min7090164.
Santos, A., Mota, M.A.D.L., Kern, H.P., Fauth, G., Paim, P.S., Netto, R.G., Sedorko, D., Lavina, E.L.C., Krahl, G., Fallgatter, C., Silveira, D.M., Aquino, C.D., Santos, M.O., Baecker-Fauth, S., Vieira, C.E.L., 2022. Earlier onset of the Early Cretaceous Equatorial humidity belt. Global and Planetary Change 208, 103724. https://doi.org/10.1016/j.gloplacha.2021.103724.
Scherer, C.M., Mello, R.G., Ferronatto, J.P., Amarante, F.B., Reis, A.D., Souza, E.G., Goldberg, K., 2020. Changes in prevailing surface-palaeowinds of western Gondwana during Early Cretaceous. Cretaceous Research 116, 104598. https://doi.org/10.1016/j.cretres.2020.104598.
Schmidt, C.J., Astini, R.A., Costa, C.H., Gardini, C.E., Kraemer, P.E., 1995. Cretaceous rifting, alluvial fan sedimentation, and Neogene inversion, southern Sierras Pampeanas, Argentina. In: Tankard, A.J., Soruco, R.S., Welsink, H.J. (Eds.), Petroleum Basins of South American. AAPG Memoirvol. 62. https://doi.org/10.1306/M62593C16.
Singer, A., 1979. Palygorskite in sediments: detrital, diagenetic or neoformed - a critical review. Geologische Rundschau 68 (3), 996–1008. https://doi.org/10.1007/BF02274683.
Singer, A., 1984a. The paleoclimatic interpretation of clay minerals in sediments—a review. Earth-Science Reviews 21 (4), 251–293. https://doi.org/10.1016/0012-8252(84)90055-2.
Singer, A., 1984b. Pedogenic palygorskite in the arid environment. In: Singer, A., Galan, E. (Eds.), Palygorskite – Sepiolite: Occurrences, Genesis and Uses. Developments in Sedimentologyvol. 37. Elsevier, pp. 169–176. https://doi.org/10.1016/S0070-4571(08)70036-0.
Singer, A., Norrish, K., 1974. Pedogenic palygorskite occurrences in Australia. American Mineralogist. Journal of Earth and Planetary Materials 59 (5–6), 508–517.
Skelton, P.W., Spicer, R.A., Kelley, S.P., Gilmour, I., 2003. The Cretaceous World. Cambridge University Press (360 pp.).
Smith, M.E., Carroll, A.R., 2015. Stratigraphy and Paleolimnology of the Green River Formation, Western USA. Springer (359 pp.).
Sousa, E.D.S., Júnior, G.R.S., Silva, A.F., de AM Reis, F., de Sousa, A.A., Cioccari, G.M., Capilla, R., de Souza, I.V.A.F., Imamura, P.M., Rodrigues, R., Lopes, J.A.D., de Lima, S.G., 2019. Biomarkers in Cretaceous sedimentary rocks from the Codó Formation-Parnaíba Basin: Paleoenvironmental assessment. Journal of South American Earth Sciences 92, 265–281. https://doi.org/10.1016/j.jsames.2019.03.025.
Suarez, M., Bell, C.M., 1987. Upper Triassic to Lower Cretaceous continental and coastal saline lake evaporites in the Atacama region of northern Chile. Geological Magazine 124 (5), 467–475. https://doi.org/10.1017/S0016756800017040.
Taylor, S.R., McLennan, S.M., 1985. The Continental Crust: Its Composition and Evolution. Blackwell Publishing (328 pp.).
Technisch Physiscge Dienst, 1966. Delft, The Netherlands. ICDD Graint-in-Aid.
Teles, M.S.L., Berthou, P., 1995. Estudo dos argilominerais das Bacias do Araripe, Rio do Peixe, Barro e Padre Marcos no Nordeste do Brasil e geoquímica orgânica das Formações Santana e Rio da Batateira na Bacia do Araripe. Universidade Federal do Rio de Janeiro (M.Sc. thesis.).
Thiry, M., 2000. Palaeoclimatic interpretation of clay minerals in marine deposits: an outlook from the continental origin. Earth-Science Reviews 49 (1–4), 201–221. https://doi.org/10.1016/S0012-8252(99)00054-9.
Thiry, M., Jacquin, T., 1993. Clay mineral distribution related to rift activity, sea-level changes and paleoceanography in the Cretaceous of the Atlantic Ocean. Clay Minerals 28 (1), 61–84. https://doi.org/10.1180/claymin.1993.028.1.07.
Tobia, F.H., Mustafa, B.H., 2016. Geochemistry and mineralogy of the Al-rich shale from Baluti Formation, Iraqi Kurdistan region: implications for weathering and provenance. Arabian Journal of Geosciences 9 (20), 1–23. https://doi.org/10.1007/s12517-016-2762-6.
Tosca, N.J., 2015. Geochemical pathways to Mg-silicate formation. In: Pozo, M., Galán, E. (Eds.), Magnesian Clays: Characterization, Origin and Applications. Digilabs, Bari, Italy, Madrid Basin (Spain), pp. 283–329.
Tosca, N.J., Masterson, A.L., 2014. Chemical controls on incipient Mg-silicate crystallization at 25 C: Implications for early and late diagenesis. Clay Minerals 49 (2), 165–194. https://doi.org/10.1180/claymin.2014.049.2.03.
Trauth, N., 1977. Argiles évaporitiques dans la sédimentation carbonatée continentale et épicontinentale tertiaire. Bassins de Paris, de Mormoiron et de Salinelle (France), Jbel Ghassoul (Maroc). Sciences Géologiques, bulletins et mémoiresvol. 19 (195 pp.).
Tutolo, B.M., Tosca, N.J., 2018. Experimental examination of the Mg–silicate–carbonate system at ambient temperature: implications for alkaline chemical sedimentation and lacustrine carbonate formation. Geochimica et Cosmochimica Acta 225, 80–101. https://doi.org/10.1016/j.gca.2018.01.019.
Vanderstappen, R., Verbeek, T., 1959. Présence d'analcime d'origine sédimentaire dans le Mésozoïque du bassin du Congo. Bulletin de la Societe Belge de Geologie 68, 417–421. https://doi.org/10.1016/0009-2541(72)90057-5.
Vasconcelos, A.M., Ribeiro, J.A.P., Colares, J.Q.S., Gomes, I.P., Forgiarini, L.L., Medeiros, M.F., 2004. Folha Teresina SB.23. In: Schobbenhaus, C., Gonçalves, J.H., Santos, J.O.S., Abram, M.B., Leão Neto, R., Matos, G.M.M., Vidotti, R.M., Ramos, M.A.B., de Jesus, J.D.A. (Eds.), Carta Geológica do Brasil ao Milionésimo, Sistema de Informações Geográficas. Programa Geologia do Brasil. CPRM, Brasília (CD-ROM).
Vaz, P.T., Rezende, N.G.A.M., Wanderley Filho, J.R., Travassos, W.S., 2007. Bacia do Parnaíba. Boletim de Geociencias da Petrobras 15 (2), 253–263.
Velde, B.B., Meunier, A., 2008. The Origin of Clay Minerals in Soils and Weathered Rocks. Springer (426 pp.).
Verma, S.P., Armstrong-Altrin, J.S., 2013. New multi-dimensional diagrams for tectonic discrimination of siliciclastic sediments and their application to Precambrian basins. Chemical Geology 355, 117–133. https://doi.org/10.1016/j.chemgeo.2013.07.014.
Viani, A., Gualtieri, A.F., Artioli, G., 2002. The nature of disorder in montmorillonite by simulation of X-ray powder patterns. American Mineralogist 87 (7), 966–975. https://doi.org/10.2138/am-2002-0720.
Vieira, R.A.B., Mendes, M.P., Vieira, P.E., Costa, L.A.R., Tagliari, C.V., Bacelar, A.P., Feijó, F.J., 1994. Bacias do Espírito Santo e Mucuri. Boletim de Geociencias da Petrobras 8 (1), 191–202.
Visser, J.N., Young, G.M., 1990. Major element geochemistry and paleoclimatology of the Permo–Carboniferous glacigene Dwyka Formation and postglacial mudrocks in southern Africa. Palaeogeography, Palaeoclimatology, Palaeoecology 81 (1–2), 49–57. https://doi.org/10.1016/0031-0182(90)90039-A.
Voo, R., 1993. The opening of the Atlantic Ocean. Paleomagnetism of the Atlantic, Tethys and Iapetus Oceans. Cambridge University Press, Cambridge, pp. 123–142.
Warr, L.N., 2020. Recommended abbreviations for the names of clay minerals and associated phases. Clay Minerals 55 (3), 1–4. https://doi.org/10.1180/clm.2020.30.
Weaver, C.E., 1984. Origin and geologic implications of the palygorskite deposits of SE United States. In: Singer, A., Galan, E. (Eds.), Palygorskite–Sepiolite: Occurrences, Genesis and Uses. Developments in Sedimentologyvol. 37. Elsevier, pp. 39–58. https://doi.org/10.1016/S0070-4571(08)70028-1.
Weaver, C.E., 1989. Clays, Muds, and Shales. Elsevier (837 pp.).
Weaver, C.E., Beck, K.C., 1977. Miocene of the SE United States: a model for chemical sedimentation in a peri-marine environment. Sedimentary Geology 17 (1–2), IX-234. https://doi.org/10.1016/0037-0738(77)90062-8.
Weaver, J.N., Brownfield, M.E., Bergin, M.J., 1990. Coal in sub-Saharan-African countries undergoing desertification. Journal of African Earth Sciences (and the Middle East) 11 (3–4), 261–271.
Whitney, D.L., Evans, B.W., 2010. Abbreviations for names of rock-forming minerals. American Mineralogist 95 (1), 185–187. https://doi.org/10.2138/am.2010.3371.
Wilson, M.D., Pittman, E.D., 1977. Authigenic clays in sandstones; recognition and influence on reservoir properties and paleoenvironmental analysis. Journal of Sedimentary Research 47 (1), 3–31. https://doi.org/10.1306/212F70E5-2B24-11D7-8648000102C1865D.
Winter, W.R., Jahnert, R.J., França, A.B., 2007. Bacia de Campos. Boletim de Geociencias da Petrobras 15 (2), 511–529.
Wipki, M., Germann, K., Schwarz, T., 1993. Alunitic kaolins of the Gedaref region (NE-Sudan). Geoscientific Research in Northeast Africa. CRC Press, pp. 509–514.
Wright, V.P., 2020. The mantle, CO_2 and the giant Aptian chemogenic lacustrine carbonate factory of the South Atlantic: some carbonates are made, not born. Sedimentology 69 (1), 47–73. https://doi.org/10.1111/sed.12835.
Wunderlin, C.A., Collo, G., Ezpeleta, M., Carbonell, V.V.R., Nóbile, J.C., Ciccioli, P.L., Faudone, S., 2022. Authigenic and detrital clay minerals as indicators of paleoenvironmental and postdepositional evolution in a Cretaceous–Cenozoic succession from argentine Central Andes. Sedimentary Geology 437, 106179.
Young, R.A., 1993. The Rietveld Method: 5. International Union of Crystallography (312p.).
Zalán, P.V., Romeiro-Silva, P.C., 2007. Bacia do São Francisco. Boletim de Geociencias da Petrobras 15 (2).